EPRI
Electric Power
Research Institute

Topics:
Heat rejection
Cooling towers
Cooling towers—plumes
Computer codes
Visible plumes
Seasonal/annual impacts

EPRI CS-3403-CCM
Project 906-1
Computer Code Manual
April 1984

User's Manual: Cooling-Tower-Plume Prediction Code

Prepared by
Argonne National Laboratory
Argonne, Illinois

User's Manual: Cooling-Tower-Plume Prediction Code

A computerized methodology for predicting seasonal/annual impacts of visible plumes, drift, fogging, icing, and shadowing from single and multiple sources

---

CS-3403-CCM
Research Project 906-1

Computer Code Manual, April 1984

Prepared by

ARGONNE NATIONAL LABORATORY
9700 South Cass Avenue
Argonne, Illinois 60439

Principal Investigators
A. J. Policastro
L. Coke
M. Wastag

Subcontractors

UNIVERSITY OF ILLINOIS AT URBANA
Department of Mechanical Engineering
144 Mechanical Engineering Building
Chicago, Illinois 61801

Principal Investigators
W. Dunn
P. Gavin
B. Boughton

UNIVERSITY OF ILLINOIS AT CHICAGO
Chicago Circle
Chicago, Illinois 60680

Principal Investigator
R. A. Carhart

Prepared for

Electric Power Research Institute
3412 Hillview Avenue
Palo Alto, California 94304

EPRI Project Manager
J. A. Bartz
Heat, Waste, and Water Management Program
Coal Combustion Systems Division

Section 2

THE SEASONAL/ANNUAL METHODOLOGY FOR PREDICTION OF VAPOR PLUMES, DRIFT DEPOSITION RATES, FOGGING, ICING, AND SHADOWING

SOURCES OF DATA USED IN PREDICTION OF SEASONAL/ANNUAL IMPACTS

Preparation of quantitative estimates of the seasonal/annual impacts of cooling towers requires substantial amounts of data concerning the physical features of the site, the meteorology of the site and the cooling towers to be used. The physical aspects of the site are readily available from U.S. Geological Survey topographical maps and from satellite and aerial photographs. The operating characteristics of the tower are usually available from manufacturer's performance curves or from previous measurements on similar towers. The potential sources of meteorological data and their attributes are as follows.

(a) On-site meteorological tower data

The proposed site will often have a 1- or 2-year record of meteorological data continuously measured and available on an hourly basis from a meteorological tower. Although efforts are being made to standardize this type of data, the location, number and kind of measurements available vary widely. Typically, one may encounter two levels (e.g., 10 and 50 m) of wind speed and direction (cup or vane anemometer), dry-bulb temperature (thermistor or thermocouple) and humidity measurements (dew-point instrument). The accuracy of these data is generally good as the equipment used is often well calibrated and reasonably sophisticated. The fraction of missing data is usually low (<10%). The main limitations of these data are the small number of measurement heights over the range of interest, the fact that the measurement heights are often well below plume level and the shortness of the record period (1 year is usually insufficient to define the climatology of the site).

(b) Ground-level data available from the U.S. National Weather Service

The U.S. National Weather Service collects and records ground-level (30-foot level) data at most major airports in the U.S. These data can be obtained on magnetic computer tape covering nearly any specific period. Five years is usually accepted as representative of the long-term climatology of the site, although longer periods are usually available, if needed. A major limitation is that the single measurement height is well below the plume; extrapolation to plume level is difficult. Moreover, the measurements are typically rather crude. For example, dry-bulb and wet-bulb temperatures are recorded to the nearest degree Fahrenheit, wind direction is recorded in terms of one of 16 quarter-quadrant directions, etc. The data also include a number of human interpretations such as cloud cover in tenths, heights of significant cloud levels, etc. Often a sizable fraction of the data are missing or unusable, requiring longer record periods to satisfactorily define the climatology. In addition to these difficulties, the question of similarity between the measurement site and the plant site always remains. Unfortunately, these data are quite often the best available.

(c) Upper air data available from the U.S. National Weather Service

The National Weather Service also records upper air data using released radiosondes at many of the larger airports in the U.S. These data are recorded twice daily at noon and midnight Greenwich Mean Time. Although the distance to the nearest upper-air measurement site may be great and the measurement times may be poorly suited to the needs of an environmental impact assessment, these upper air soundings are often the only source of measured data on the inversion height experienced by a rising plume. Holzworth (see Appendix A) provides a tabulation of mean seasonal and annual mixing heights which may be used as an alternative to the NWS bi-daily measurements.

(d) Intensive on-site meteorological data

A good complement to the data from the on-site meteorological tower is data gathered during one-to-two week intensive surveys conducted at selected periods throughout the year. These data, which are rarely available, are the most reliable vehicle to define the upper-air structure of the site.

An important first step in making a reliable assessment of potential cooling tower impacts is the development of a representative and meaningful base of meteorological

data from the available sources. Important characteristics of the available measurements are that they (a) are large in number (tens of thousands of individual records), (b) may contain a large fraction of missing or otherwise unusable data, (c) may be limited in accuracy and detail, and (d) constitute a wide spectrum of data types. Once the data base is established, this high volume of information must be translated into simple yet meaningful descriptions of plume behavior using a mathematical model with established validity.

PREVIOUS METHODS OF PROVIDING PREDICTIONS OF SEASONAL/ANNUAL PHYSICAL IMPACTS OF COOLING TOWERS

The methodology presented in this manual has evolved from three earlier methods, each of which has, in succession, added a new level of sophistication to the analysis.

The first method used may be loosely referred to as the "prior experience" approach. Here, assessments are based solely on previous operational experience with similar towers in similar climates. This method avoids mathematical models and is relatively inexpensive to apply. However, in addition to the obvious limitation inherent in such subjective evaluations, there is always the problem of finding a sufficiently similar operating plant. In many cases, interpretation overshadows fact and a highly trained expert is required to make the most reasonable interpretations. Licensing boards often frown on conclusions and recommendations reached primarily on the basis of opinion, even that of experts.

The second method represents the opposite philosophy. Here, a large data base encompassing an on-site measurement tape or a NWS ground-level measurement tape is used. For each measurement record (e.g., hourly value), simple formulas are employed to calculate gross plume properties and the results are added to running totals. After all data have been processed, averages are computed and presented in tabular or graphical form. The best known implementation of this approach is the ORFAD code (1) developed by investigators at Oak Ridge National Laboratory. The ORFAD philosophy provides quantitative estimates of impact without subjective input, thus assuring consistency between the results of different groups using the code for site evaluation. The need to repeat computations for every data record precludes the use of any but the simplest plume model. Moreover, these formulas were shown (2-4) to compare poorly with observations of real plumes and thus the

reliability of the end result is questionable. Moreover, knowledge of extreme plume behaviors is lost through the cumulative effects of the total data base.

Recognizing the limitations of the two earlier methods, the developers of the KUMULUS model (5) devised a scheme to produce a set of typical meteorological conditions, based on the widely accepted hypothesis that only a limited number of significantly different plumes actually exist at a particular site. This approach allows a validated plume model to be used (in this case, the developers' own) and, further, permits both average and extreme behaviors to be identified. To obtain the typical meteorological input, each data record is classified according to ranges in wind speed, humidity, temperature and lapse rate. For example, categories are determined, in part, by dividing the maximum ambient temperature to 1000 m elevation into five discrete intervals or bins as follows: $T \leqq 7.5\ ^{\circ}C$, $-7.5\ ^{\circ}C < T \leqq 0\ ^{\circ}C$, $0\ ^{\circ}C < T \leqq 10\ ^{\circ}C$, $10\ ^{\circ}C < T \leqq 20\ ^{\circ}C$, and $20\ ^{\circ}C < T$. Similar divisions in the remaining variables produces 400 total bins into which the data records can be sorted. In one application of this method (5), the total number of plume categories was reduced to 80 typical cases and 10 extreme cases. The final set of 90 cases is then simulated using validated plume and drift models.

Although the KUMULUS approach represents a significant advance in technique, it still suffers from several deficiencies. First, the range in behaviors within a given category differs from category to category and is generally unknown a priori. No assurance exists that two plumes from two different categories will be any less similar than two from the same category. Second, the selection of parameter ranges is difficult and our experience indicates that plume categories also depend on tower characteristics (not included in the KUMULUS category scheme) and the particulars of the site.

PRESENT METHOD

The present method is similar to the previously discussed KUMULUS approach in that typical sets of input data are used in conjunction with a validated plume model (i.e., a model whose limits of accuracy have been established and found satisfactory) to produce a number of representative plumes. The present method differs from the previous approach in that categories are based on nondimensional parameters which have been shown to correlate well with plume length and rise, rather than on simple ranges in the dimensional meteorological data.

Nondimensional Plume Parameters

The basic conceptualization of the problem is shown in Fig. 2-1. Here, the governing dimensional parameters are identified. Note that the ambient has been idealized in terms of a power-law wind profile, a linear temperature profile and a constant dew-point depression. This simple conceptualization is satisfactory for identifying the basic scaling relationships of plume dispersion. These parameters can be reduced to four nondimensional groups which along with n, the wind exponent, fully define the plume within the context of our simple conceptualization. The nondimensional groups are as follows.

Richardson Number:

$$Ri = \frac{\Delta\rho g D}{\rho W_o^2}$$

The Richardson number indicates the relative amount of buoyancy of the plume.

Crossflow Velocity Ratio:

$$k = U/W_o$$

The crossflow velocity ratio determines the relative importance of the crossflow.

Stability Parameter:

$$S = \frac{D^2 g}{U^2 T_a} \left(\frac{dT}{dz} + \Gamma_a\right)$$

Here, Γ_a is the adiabatic lapse rate. The stability parameter characterizes the stratification of the ambient.

Volume Dilution to Saturation:

V_* is determined by solving the equation

$$(V_*-1)\ \phi + \phi_o = \phi_{sat}\ ((V_*-1)\ T+T_o)$$

subject to the constraint that $V_* > 1$, where $\phi_{sat}\ (\tau)$ is the saturation mixing ratio of water vapor at temperature τ. V_* can be interpreted as the total volume

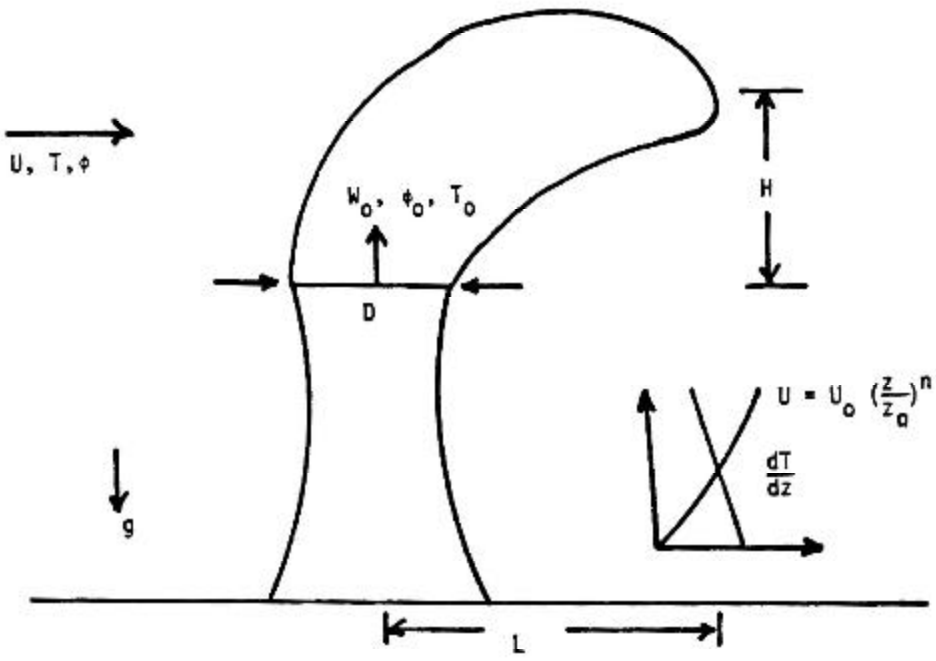

Parameters:

D = exit diameter

W_o = exit velocity

ϕ_o = exit mixing ratio

T_o = exit temperature

U = integrated average ambient wind speed

T = integrated average ambient temperature

ϕ = integrated average ambient mixing ratio

g = acceleration of gravity

n = wind exponent

dT/dz = temperature lapse rate

dT_d/dz = dewpoint temperature lapse rate

L = visible plume length

H = visible plume rise

Figure 2-1. Conceptualization of plume problem.

to which one unit of plume air must be diluted with ambient air, such that the resulting mixture is just saturated.

Starting with these parameters and applying simple bulk mixing concepts, we can further derive two more groups which are functions of Ri, k and V_*.

Length Parameter:

$$LP = (k^2/Ri)(\sqrt{\eta} - 1)$$

where $\eta = \max [1, 2 (Ri/k)(r_*^3-1) +1]$

and $r_* = V_*/[k (V_*-1) + 1]$

Height Parameter:

$$HP = \max (r_*-1, 0)$$

We refer to these groups as the "length" and "height" parameter, since our analysis indicates that they should correlate with the nondimensional visible plume length $L_* = L/D$ and the nondimensional visible plume rise $H_* = H/D$, respectively. To test this hypothesis, we compare in Figs. 2-2 and 2-3 the nondimensional plume length and plume rise with their corresponding indicators using observed plume data from 3 sites: Chalk Point, Lünen and Paradise. Considering the uncertainty in the data and the simplicity of our analysis, we find a high degree of correlation between observed plume behavior and our two dimensionless indicators. The few cases of large discrepancy turn out to be also very difficult to predict using more sophisticated plume models. Thus, we believe that these nondimensional parameters provide a reliable means of categorizing plumes for the purposes of seasonal and annual impact assessments.

To extend this method of categorizing plumes to multiple-source configurations, we establish the concept of an "effective" source diameter. The effective source diameter may be based on a single cell, a tower, a cluster of towers or the sum of all cells and towers combined. The choice is based on which grouping is expected to be most representative of plume interaction given the often-complex geometry of the site. Based on sensitivity studies made with the multiple tower plume and drift codes, we find that the choice of most representative effective source diameter is not crucial for the purpose of selecting categories so long as plume

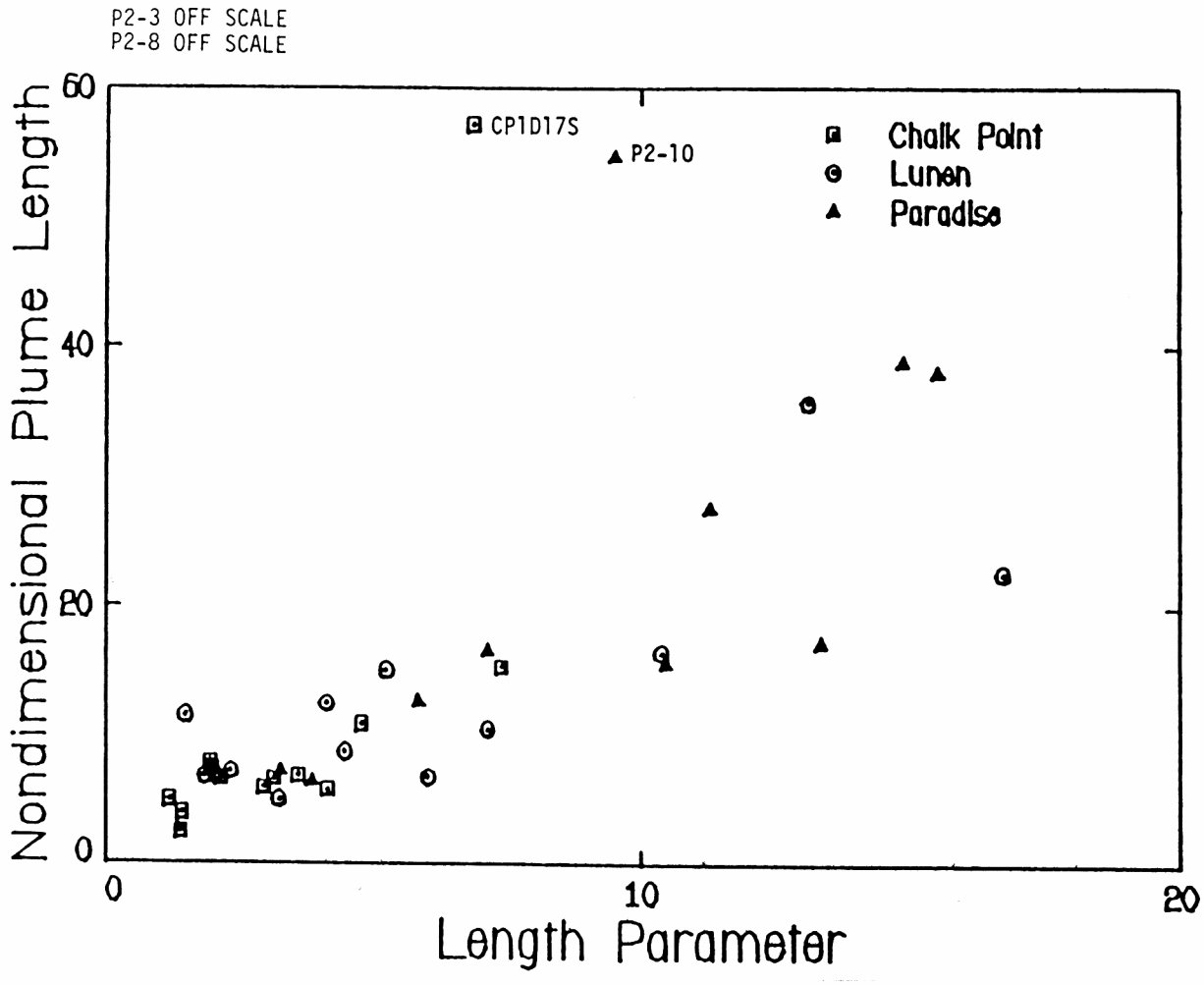

Figure 2-2. Comparison of nondimensional length parameter with nondimensional observed visible plume lengths at three sites.

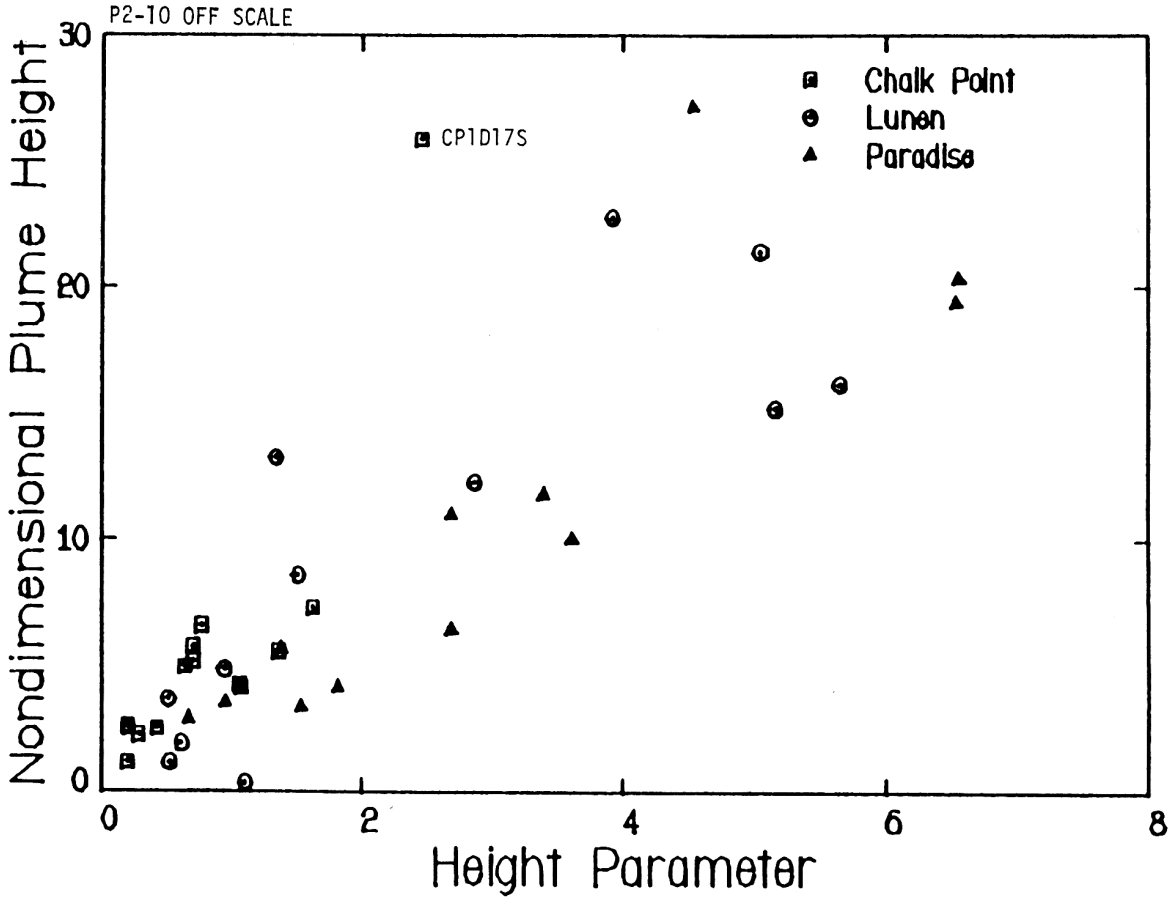

Figure 2-3. Comparison of nondimensional height parameter with nondimensional observed visible plume rise at three sites.

exit temperature and velocity are correctly computed. The following rules of thumb may be used in selecting the most representative effective-source diameter.

1. The individual cells (exit areas) of both linear and circular mechanical-draft towers should be combined together on a tower-by-tower basis.

2. Towers (exit areas) should be combined together if the separation distance between centers is less than

   (a) 5-10 tower diameters for natural-draft cooling towers,

   (b) 2-3 effective tower diameters for circular mechanical-draft cooling towers or

   (c) 2-3 times the long dimension of the tower structure for linear mechanical-draft cooling towers.

The effective diameter is computed so as to maintain the same total area of outflow. Thus, for N cells of diameter D, the effective diameter D_{eff} is given by

$$D_{eff} = \sqrt{N}\, D.$$

Another addition necessary for treating multiple-source configurations involves the definition of representative wind directions. In this manner, the sixteen wind directions present on the meteorological data tape are grouped together so as to minimize the number of possible variations which must be considered. For an example of three natural-draft cooling towers oriented in a straight line, the representative wind directions might be designated (1) crossflow, (2) 45 degrees with respect to tower axis and (3) inline. Each of the 16 traditional wind directions is then identified with one of these representative directions as illustrated in Fig. 2-4. In this example, the number of plume categories is increased by a factor of 3 when the effects of directionality are included. The number of representative wind direction will rarely, if ever, exceed 5. A more complete discussion of the selection of representative wind directions is given in Appendix C.

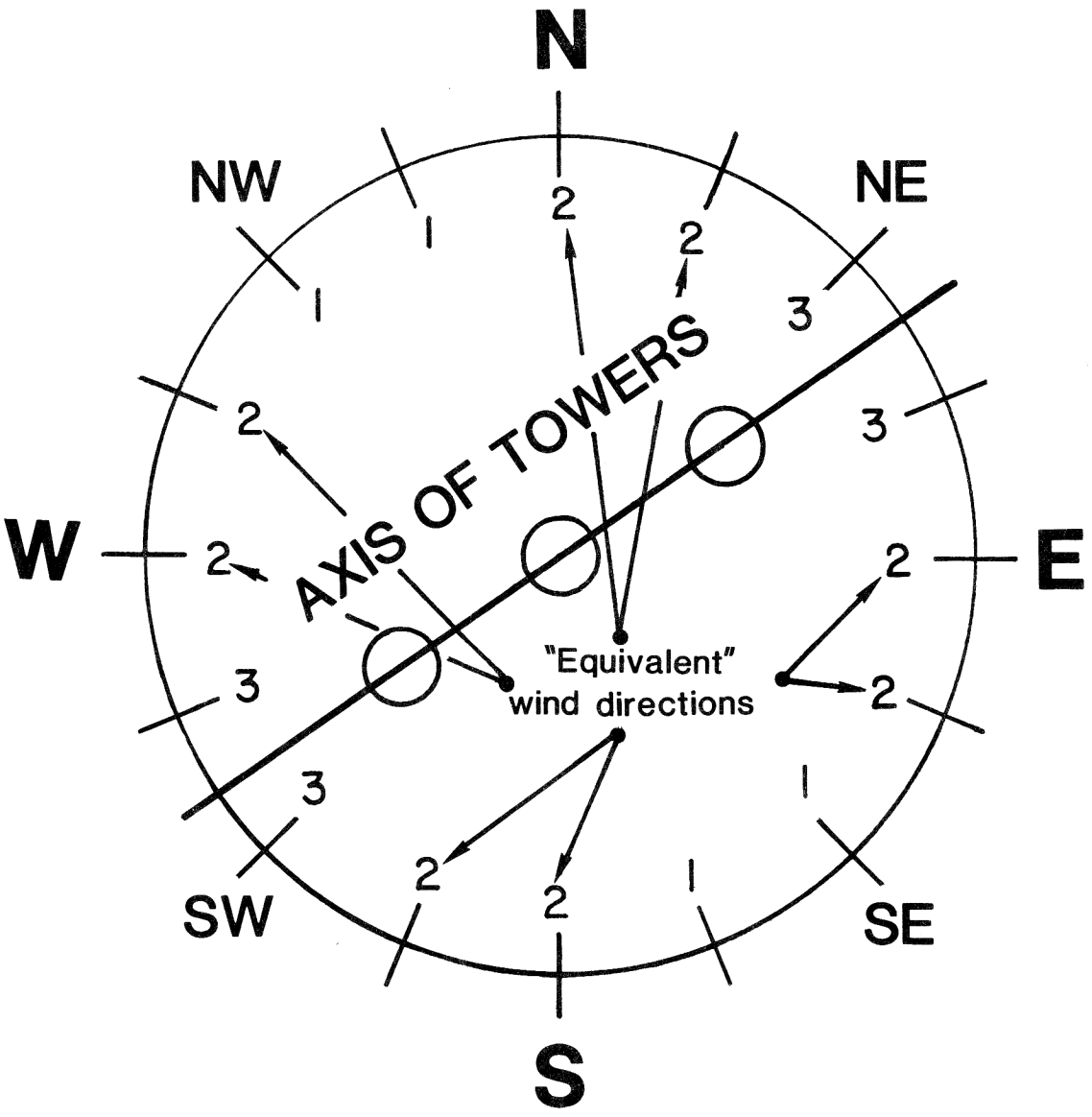

Figure 2-4. Example of the use of characteristic wind directions for modeling plumes from a site with three colinear natural-draft cooling towers.

Structure of the Seasonal/Annual Methodology

The steps in the application of this methodology are as follows:

1. Development of enhanced data base including statistical analysis of data base and category selection (PREPROCESSOR Program)

2. Simulation of representative plumes (PLUME Program)

3. Tabulation of frequencies (TABLES Program)

4. Plotting of isopleths (PAGEPLOT Program)

The development of the enhanced data base (step 1) consists of three major subtasks. In the first subtask, each record on the weather tape is read and unnecessary information and incomplete or otherwise unusable records are eliminated. For each valid record, cooling tower exit variables (temperature, velocity) are computed. The nondimensional parameters listed earlier are also computed.

The second subtask of step 1 involves a statistical analysis of the data base as it is being enhanced. Among the information provided in a hard copy output of the PREPROCESSOR Program are tables of frequencies of occurrence in different wind directions of selected parameter ranges for relative humidity, wind speed, dew point temperature, dry bulb temperature, k value (ratio of wind speed to exit velocity), V_*, LP, HP, etc. From such statistical outputs, the user can develop a better understanding of the climatology and expected plume behavior at the site.

Once the full tape is read, the third subtask of step 1 involves the choice of categories based on the statistics created. The most important parameter for determining the categories is length parameter. Categories are chosen based primarily on ranges in the value of LP. Secondary parameters employed in refining category selection are k, stability class and mixing height. Categories are selected so that all categories are roughly equally populated. In a typical site simulation, 35 categories may be created for plume/drift calculation and 10 extra categories are created to handle cases for which fogging/icing are expected to occur. For each of the 35 + 10 categories, a representative set of ambient and tower exit conditions is generated to represent that category.

In step 2, the PLUME code is used to make predictions for each case chosen by the PREPROCESSOR program for each representative wind direction. Thus, assuming 35 plume and drift categories, 10 fogging and icing categories and 3 representative wind directions, the total number of plume cases which must be simulated becomes 135 = 3x (35 + 10).

In step 3, the TABLES program determines the frequency of occurrence of each category as a function of wind direction and season through a second and final reading of the augmented meteorological data base produced by the PREPROCESSOR. The frequency of occurrence statistics are, in turn, combined with the predictions of the PLUME code for each plume category to obtain tables of predicted impact by wind direction, distance from towers and season.

The fourth and final step of the prediction process involves the use of the PAGEPLOT program to produce graphical interpretations of the TABLES output in the form of line-printer "plots".

Schematization of the Ambient Meteorology and Cooling Towers

Based on the limited meteorological and tower data available for a site simulation, a number of assumptions are required in order to fill the data gaps. The most important are those needed to establish ambient profiles. Since the meteorological tapes provide either ground-level data (TDF-14 or CD-144 tapes) or data from a meteorological tower (typically three elevated levels), assumptions must be made to extend the ambient profiles to plume rise heights as needed by the plume program.

The assumptions below are for a TDF-14 or CD-144 meteorological data tape.

1. stability class (from which temperature lapse rate is known) is based on measured wind speed, ceiling height, cloud cover, solar elevation angle and time of day.

2. exponent of wind-speed power-law formula is based on stability class.

3. ambient humidity profile is obtained from the assumption that the dew-point lapse rate is equal to the dry-bulb temperature lapse rate. In this way, the dew-point depression is held constant with height. Ground-level dew-point and dry-bulb temperatures are known from data on the meteorological tape.

The following assumptions are for meteorological data tapes in NRC format:

a. temperature lapse rate is computed directly from the measured temperatures at the top and bottom levels of the measured data, if available; otherwise, from other pairs of levels as a variable.

b. wind-speed power-law profile is computed from two wind speeds measured at different elevations.

c. dew-point lapse rate is also taken equal to the dry-bulb temperature lapse rate in order to obtain the humidity profile.

For the computation of tower exit velocity and temperature, a simple thermal performance model for the cooling tower is employed which assumes a constant air mass flow rate through the tower over time. With this knowledge of the exit air flow, a simple enthalpy balance on the cooling tower is used to compute the tower exit temperature on an hour-by-hour basis as records are read in from the weather tape. Exit air velocity is then computed from the known mass flow rate and effluent density.

Our computation of stability class and wind speed power law exponent for the ground-level weather tapes is carried out within the PREPROCESSOR program based on methods used in the CRSTER Model (6). The CRSTER Model is widely utilized in making air quality calculations. A final comment should be made on the use of mixing heights. If an upper air weather tape is also available, it is used to provide twice-daily mixing heights at the location of the upper air station. An algorithm (from CRSTER) is used to compute mixing height on an hour-by-hour basis. The hourly mixing height is considered the upper bound to any plume predicted with the LP, HP formulas. However, in the PLUME program, a single value of mixing height is used (annual average for the site) from Holzworth (7) above which an isothermal atmosphere is assumed.

Submodel for Visible Plume Rise and Salt Drift Deposition

The theory and philosophy behind the development of our plume rise and drift deposition models is given in detail in Refs. (8-13). The reader is urged to refer to those reports for details on the theoretical development and validation

of the single- and multiple-source plume and drift models. Only a short summary is given here.

(a) visible plumes

The model improvement work presented in the five-volume report (8-13) builds on our earlier evaluation of the theory and performance of over 30 plume and drift models that have been available to utilities for preparation of their Environmental Reports. That earlier study (2-4), carried out for the U.S. Nuclear Regulatory Commission during the period of 1976 to 1978, was limited to the ad hoc evaluation of models to satisfy the immediate needs of the Commission staff and did not permit the modification of models to improve their predictive capability. The evaluation revealed that no single model predicted well over the full range of available data, although certain modeling approaches emerged as clearly superior to others. These results, coupled with a growing availability of field and laboratory data suitable for model development, made it possible to identify several key steps toward model improvement. The gap which existed between the predictive capability of even the best of the available models and the body of observational data could be significantly reduced. Under EPRI sponsorship, a two-year program was undertaken to develop the best modeling hypotheses and new models which could be confidently used to predict the behavior of cooling tower plumes and drift.

Our testing and evaluation of previous plume rise models revealed the following areas of significant weakness in existing models:

(a) proper balance between momentum transfer and buoyancy
(b) treatment of moisture thermodynamics
(c) tower wake effects
(d) effects of atmospheric dilution

Recognizing the above problem areas, we formulated a generic integral plume model to allow us to freely compare a variety of modeling hypotheses. As do all integral models, our model numerically solves a set of ordinary differential equations governing plume properties such as mass flow rate, temperature and vapor content as a function of distance along the plume trajectory. Modeling hypotheses were selected on the basis of providing the best qualitative agreement with the systematic behavior evident in the data. Specific values of the modeling coefficients were

then chosen to provide the best overall agreement with the total data base including both laboratory and field data from a wide variety of configurations. The model was also tested with new data not part of the calibration base and found to perform well. To assess the relative performance of the ANL model, we have compared it with 5 other models which can handle both single and multiple tower configurations and which were also calibrated to all of part of our data base by their developers.

In predicting visible plume rise and for application to data from single (and multiple) sources, the ANL model showed the best performance among the competing models in terms of all of our statistical measures of predictive capability. In roughly 77% of the cases, the ANL model predicts visible plume rise within a factor of 2. The model showed its greatest weakness for short plumes, cases for which errors in prediction are more acceptable. However, given the uncertainty in the data, the superiority of the ANL model over the second best performing model (KUMULUS) is not statistically significant. Both models do well and, with respect to the field data, may be considered on a par in predicting visible plume rise.

For visible plume length, the ANL model predicts within a factor of 2 (our value for an acceptable prediction within the limits of modeling and data uncertainties) in approximately 60% for all field cases tested. Although this is only on par with the top models in terms of this single statistic, the ANL model is much less prone to gross over- or under-prediction (e.g., more than a factor of 5 in error) than the other models tested. Our model calibration procedure revealed that a significant decrease in the number of very bad predictions would come at the price of a slight decrease in the number of very good predictions. Our calibration procedure was aimed, in part, in assuring only a small number of very poor predictions. That tradeoff was acceptable and was supported by our later model validation work (14).

In comparison with single-phase laboratory data, the ANL model is clearly superior to all tested models (over the full range of single- and multiple-source data.)

The development and verification of the ANL multiple-source model is an extension of the single-source model to include a physically reasonable merging scenario and a realistic analysis of tower downwash. The model has been calibrated with a limited amount of laboratory data and verified with field data and additional laboratory data.

Our merging methodology is a modification of the treatment developed by Wu and Koh (15). The Wu-Koh method is essentially a geometric treatment in which a merging plume is represented by a finite-length slot jet capped on each end by a half-round jet. Various criteria are presented to determine the exact location at which the two plumes have merged, the shape of the merged cross-section, and the fluxes of the merged plume in relation to the fluxes of the individual plumes prior to merging. The Wu-Koh treatment of merging satisfies two important physical constraints:

(i) for cases in which the wind is directed in line with a row of sources, the plume will rise higher after merging than for the identical case in which the wind is directed normal to a row of sources.

(ii) predicted plumes begin as round plumes, merge into more elliptical shapes, and finally evolve back into a round plume.

The downwash treatment in the multiple-source model extends the methodology included in the single-source model by handling the more complex wakes produced by multiple NDCT structures and rows of MDCT cells in large circular or linear housings.

Comparisons with the multiple NDCT data from Amos and Neurath show very good plume rise predictions with only a slight tendency to underpredict rise when observed plumes are high. Predictions of visible plume length are also good with, again, a slight tendency to underpredict the very longest plumes. Among all multiple-tower models tested (5 in total), the ANL model shows the best predictive capability. For all of the 20 data cases from Gaston (two 9-cell LMDCTs), the model predicted visible plume rise and length within a factor of two, again giving considerably more accurate predictions than the other two models tested.

It must be emphasized that our goal is to achieve a model which not only can handle all situations of practical interest, but which does so without the need to recalibrate the model parameters for each new situation. The success of the ANL model in comparisons with the broad base of observational data which we have assembled supports our belief that this model can be used confidently over a wide range of applications, including large new plants with cooling towers. Clearly, our model validation was carried out largely for smaller and medium-sized sources of heat and moisture release. The only exception were our model/data comparisons for plumes from the Amos Plant (2900 MWe). A correct treatment of plume physics

augurs well for application of the model to sources that are larger (or smaller) than those used for model testing.

(b) drift deposition

Improved drift deposition models for single and multiple sources are developed starting from the single- and multiple-source plume models. A drift deposition model can be viewed as consisting of four basic submodels: plume dispersion, breakaway, evaporation, and deposition.

Our extensive analysis of droplet evaporation began with an examination of six formulations used in the available drift models. We found that the disparity among predictions was great and that many models involved simplifying assumptions that yielded significant errors in evaporation rates, distances to deposition, and final particle characteristics (3, 10). The treatments of dry particle formation from the drift drops were found to be grossly in error in terms of theory; in terms of performance, the models compared poorly with available laboratory data on particle drying rates.

Based upon the knowledge gained in the above-mentioned comparisons of existing evaporation submodels, we undertook the development of an improved analysis of drop dynamics and thermodynamics which was incorporated into our drift model. Starting from sound physical principles and calling upon previous experimental studies of drop evaporation, we have developed an analysis which avoids the arbitrary simplifications inherent in most of the earlier models. For drops reaching their final state, the present model predicts the point of deposition further from the tower than any of the other existing models tested. That result is due to the fact the the final state is actually a porous particle, a result consistent with observational data.

The improved drift model was tested with data from the 1977 Chalk Point Dye Tracer Study. This study, which provides the best data on cooling tower drift deposition presently available, involved the use of a fluorescent dye in the cooling tower/condenser water flow so as to be able to distinguish cooling tower drift deposition at the ground from other sources such as the plant stack. Model predictions of sodium and liquid deposition rate, number deposition rate of drops, and average drop diameter were compared with measured values at 500 and 1000 m from the tower. The study showed that the ANL model performed within a factor of 3 of the data with either (a) a method of breakaway which provides a continuous variation of

drop environment (Gaussian distributions of plume variables with no sharp breakaway point), or (b) the simpler criterion in which the drop adjusts suddenly from plume to ambient conditions at the point where the drop has settled below the centerline a distance equal to the local plume radius. In criterion (b) the sudden adjustment from plume to ambient conditions is the result of the drop experiencing assumed top-hat distributions of plume variables as it passes through the plume. Criterion (b) was selected for its simplicity, although both methods performed equally well.

Performance of the ANL single-source drift model may be given in terms of a rough statistic: a model succeeds in its prediction of drift at a given sampler if that prediction is within a factor of three of the measured data. If we do not distinguish between successes and failures among different deposition indicators (sodium deposition flux, number drop deposition flux, average diameter, and liquid mass deposition flux), we find that the ANL model with either of the two breakaway criteria noted above had 24 successes of 26 individual sampler comparisons. This good performance was with field data taken at downwind distances of 0.5 and 1.0 km. The single-source model is untested for distances greater than 1.0 km due to the lack of good-quality field data at those distances.

The multiple-source drift model was tested using data on ground-level sodium deposition flux taken at Pittsburg, California, a site with two mechanical-draft cooling towers of 13 cells each. The data are the best available for multiple sources, yet these data have several weaknesses. In four of the five data surveys used to test the model, the model predicts sodium deposition rate within a factor of 3 at 50% of all ground samplers.

Submodels for Ground-level Fogging and Icing

Two often-mentioned environmental effects which will occur at some sites under appropriate meteorological conditions are (a) ground fogging, and (b) deposition of rime ice on the ground and on elevated structures in the vicinity of the tower. We reviewed the literature covering the theory of natural fog production (water drop and ice crystal) and the associated deposition of rime ice under subfreezing conditions. We also reviewed the few field studies which made some attempt to measure augmentation of these natural processes by cooling towers (16). We concluded that the initiation or modification of natural fogging and icing episodes through the addition of new moisture to the ambient by cooling towers are not measurable effects. However, the impingement of a visible cooling tower plume on

the ground, or on an elevated structure, would be an observable and significant fogging (and/or icing) event. Thus, in our plume model, we have provided for the calculation of fogging and/or icing only when the visible plume makes contact with the ground.

(1) Natural-draft towers do not produce persistent ground fogging or rime ice deposition. Very transient contact of visible plume puffs with the ground has been reported at a three-tower installation at Neurath, West Germany (17) but resulted solely from downwash effects caused by the presence of buildings upwind of the towers. Natural-draft towers may, however, deposit small amounts of glaze ice at subfreezing temperatures due to drift (falling liquid water droplets) in the near field. This is particularly true if the drift eliminators are old or damaged.

(2) Circular-mechanical draft cooling towers (CMDCTs) produce some persistent ground fogging in the near field for high winds and high relative humidities. This effect will begin to occur when the wind speed exceeds the range of 10-12 m/sec, a range of wind speeds where significant recirculation effects have also been observed for CMDCTs. If the temperatures are subfreezing, this ground contact of cloud water droplets will usually produce rime ice deposition, as has been observed (18) from the dispersion of steam fog at Commonwealth Edison's Dresden cooling pond. As further experience is gained in northern climates with CMDCTs, these tentative assertions can be more fully verified.

(3) Linear-mechanical draft cooling towers (LMDCTs) produce somewhat more ground fogging and icing than do CMDCTs, and do so at lower wind speeds. Persistent ground fogging in the near field can begin to occur for wind speeds in the 8-10 m/sec range. Little information exists as to the amount of rime ice produced by these towers. However, when drift eliminators have been damaged and/or temperatures remain continually below freezing for long periods, serious glaze ice buildups from the freezing of drift droplets have been reported. (In the most notable case, at the Palisades plant in Michigan, the presence of elevated hillsides very near the plant was also a major factor in observed icing.)

In developing a mathematical model which will give quantitative predictions of fogging and icing, our primary goal was to insure that the model exhibited the above three trends. The ANL plume model has a realistic formulation of tower downwash effects which does produce good dilution and trajectory predictions under high wind conditions when downwash is important. Also, when the model is run for

high winds and high relative humidities, it predicts ground contact of the visible plume. We decided to run the model for a variety of high-humidity high-wind conditions and for a range of ambient temperatures to investigate whether it could, without significant modification, give fogging predictions satisfying conditions (1)-(3). A "standard" design LMDCT and CMDCT were used in the study (see Figures 2-5 and 2-6).

Ambient stability did not affect the model predictions significantly and was neglected in this study. Only when the predicted plume was in the tower wake did fogging predictions occur, and this region extends only tens of meters above the ground for CMDCTs and LMDCTs, so that differences in the temperature profiles between various stabilities did not have enough vertical distance to become large for the fogging and icing predictions. All of the same assumptions on meteorological conditions were made which we use in the seasonal/annual model: a constant lapse rate for vertical profiles of both ambient dry-bulb and dew-point temperatures, pressure varying hydrostatically, and a wind speed profile which follows a power law (with an exponent of 0.25 for neutral conditions). We assumed neutral stability for these runs.

The ranges of ambient parameters considered were as follows:

dry bulb temperature ... T_{DB}	-10, 0, 10, 20	degrees C
dew point depression ... DPD	0.5, 1, 2, 4, 6	degrees C
lapse rate	-0.00975	deg. C/m
wind exponent	0.25	
wind speed (CMDCT) ... U	8.3, 11, 13.8, 16.5	m/sec
(LMDCT) ... U	9, 11.3, 13.5, 15.8	m/sec

The results of the 80 test runs for the CMDCT are shown in Figure 2-7. The horizontal axis is dew-point depression in deg. C, and the vertical axis is wind speed in m/sec. The dots represent conditions for which the model predicted some near-field fogging and/or icing; the crosses represent conditions where no fog was predicted. Clearly, fogging did not occur unless the wind speed exceeded 12 m/sec a k-value exceeding 2.0 was needed to yield ground fogging.

The situation is more difficult for the LMDCT because the single-source model described here does not give as accurate a description of the actual plume as it does for the CMDCT. For an actual LMDCT in cross-flow orientation to the wind (the wind direction for which we expect the most fogging), the plume is initially

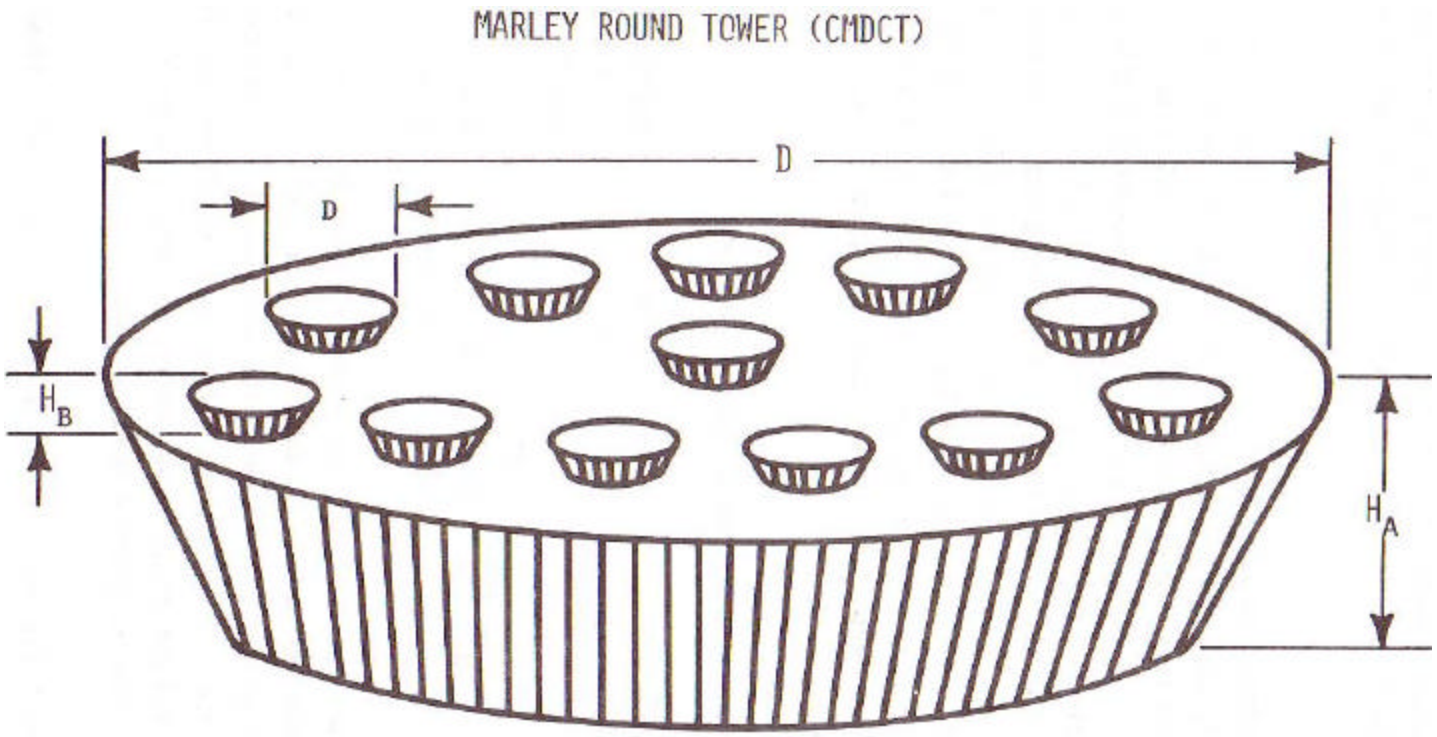

Figure 2-5. Tower geometry and exit conditions for typical circular MDCT (Marley Tower (19)).

TOWER FROM GASTON PLANT (LMDCT)

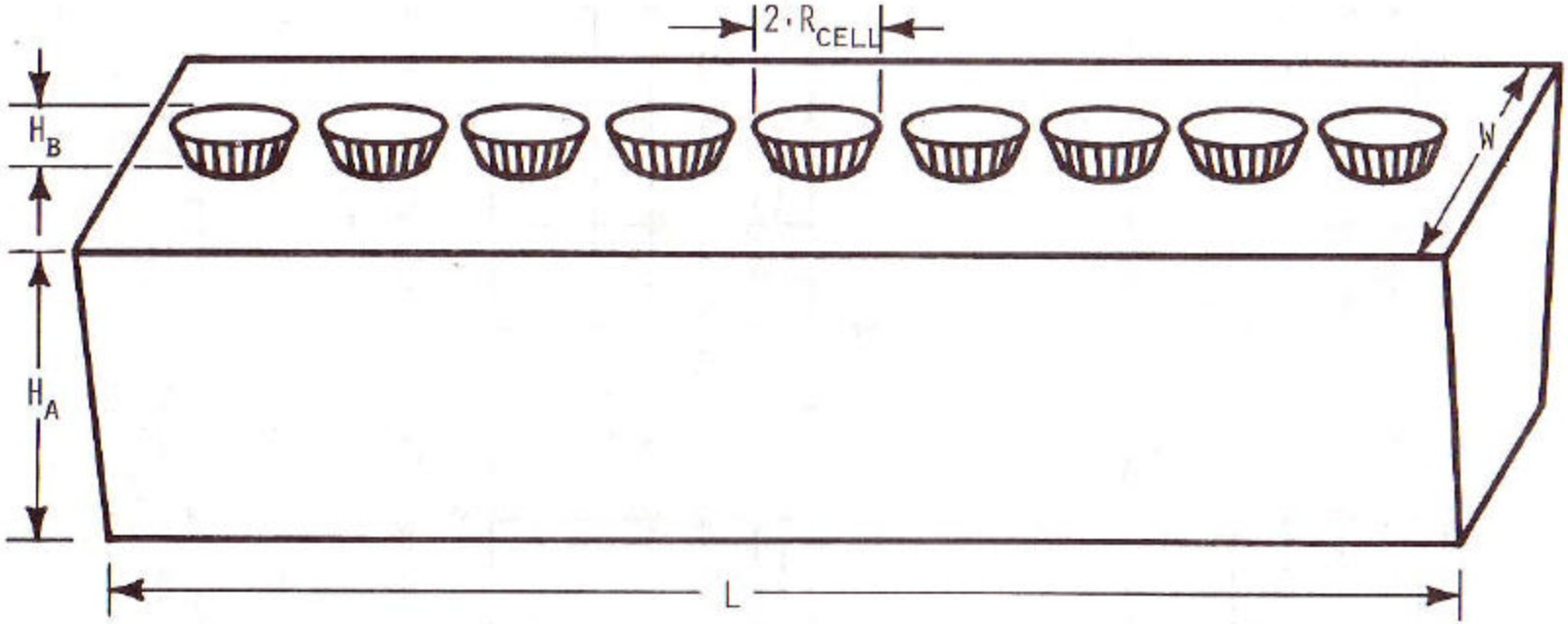

$H = H_A + H_B = 16.9$ M

$L = 98.8$ M

$W = 22.2$ M

$R_{CELL} = 4.57$ M

$W_O = 9.0$ M/S

HEAT REJECTED = 70 MW/CELL

$R_{EFF} = 13.7$ M

NINE CELLS

Figure 2-6. Tower geometry and exit conditions for typical linear MDCT (Gaston Tower (19)).

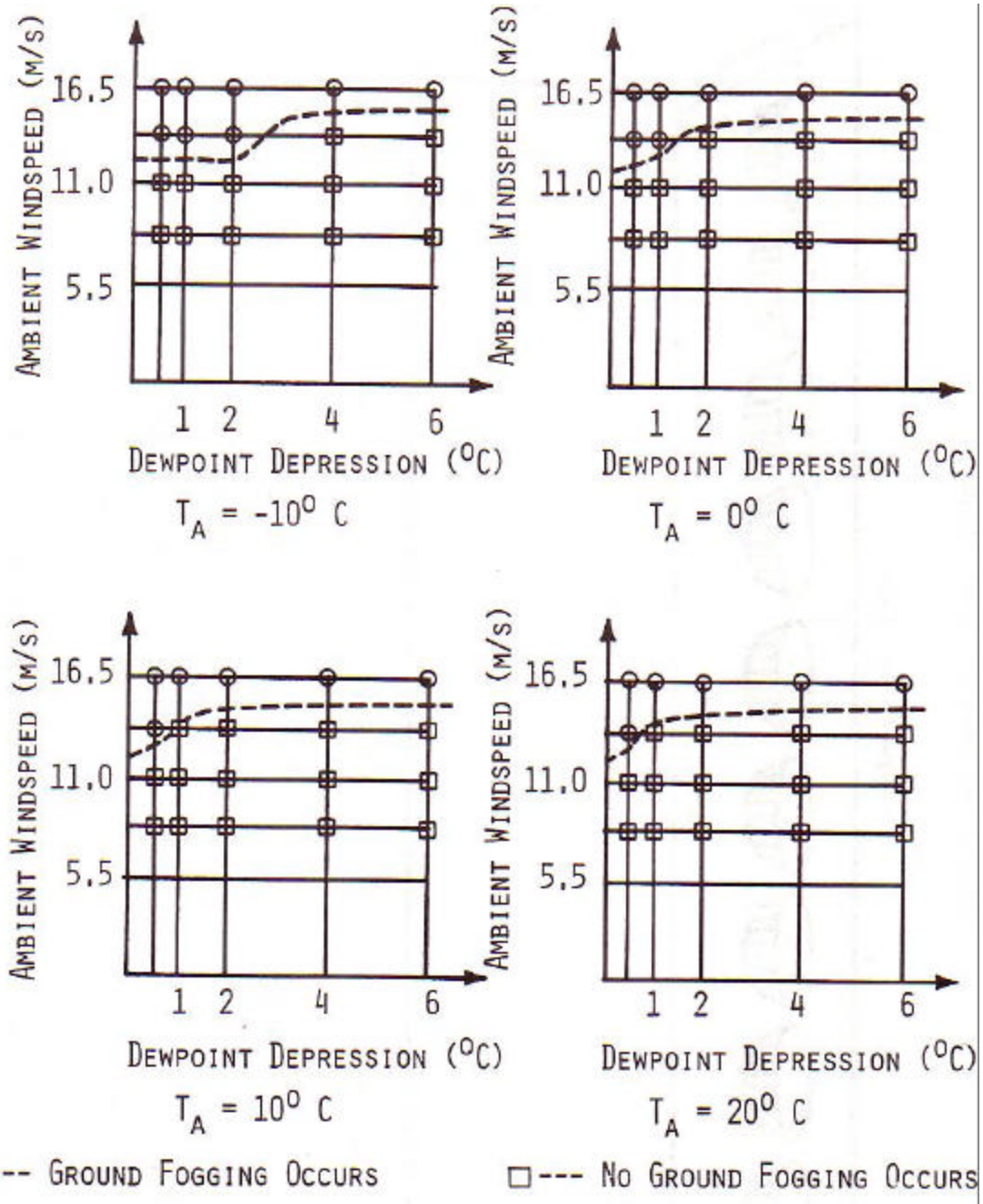

Figure 2-7. Calculation of the boundary between ground fog and no ground fog as a function of ambient wind speed, dew-point depression and ambient temperature for the standard CMDCT based on 80 test runs. The dotted lines show the approximate critical wind speed for occurrence of ground fog as a function of dew-point depression with the total heat dissipated by the tower (and the exit velocity) held constant.

very elliptical as predicted by the multiple-source model and experiences much more entrainment and pressure drag force than does the "effective source" approximation of that plume. The LMDCT plume problem then is precisely the kind of case for which the multiple-tower model is most needed.

We studied the above cases with both our multiple-source model and with the "effective-source" model, and concluded that very similar fogging events could be achieved with the single-source model if the wake entrainment and wake pressure force coefficients were increased by 50%. In this way, the single-source plume experiences the heightened mixing and bending which the actual elongated merging plume would show. Figure 2-8 presents the results of the 80 runs of the single source model with a cavity size and wake plate size typical of the actual LMDCT housing, and with the larger coefficients mentioned above.

Despite the fact that the plume exit velocity is 9 m/sec, fogging occurs for wind speeds as low as 9 m/sec at low temperatures and small dew-point depressions. As for the CMDCT, the minimum wind speed at which fogging occurs increases with ambient temperature and ambient dew-point depression. The dotted line in Fig. 2-6 shows the results of predictions with our multiple-tower code. Of course, the fogging events for the LMDCT would be less severe for other wind directions than for crossflow. However, since the maximum effects occur in pure crossflow, we can use the single-source model to select fogging/icing categories in our seasonal/annual methodology (with the wake parameters appropriate for the LMDCT in a crossflow orientation) with the knowledge that our results will be conservative.

The multiple-tower version of the seasonal/annual system of codes has incorporated within it the dependence of fogging and icing on wind direction for a LMDCT as well as for installations with multiple NDCTs, CMDCTs or LMDCTs. As for the plume predictions themselves, the user specifies a set of standard wind directions to encompass the truly different wind orientations at the site. For each fogging/icing category, the resulting ground fog (ice) pattern is calculated and stored for each of the standard wind directions. (Thus, for 3 standard wind directions, a total of 30 detailed model fogging/icing case runs are made.) In distributing and accumulating the fogging or icing for a given category and for a given meteorological wind direction, the appropriate standard wind direction prediction is used, as specified by the I(J) discussed above and in Appendix C.

For any CMDCT or LMDCT, ranges of ambient temperature, wind speed, and ambient dew-point depression have been specified which cover the conditions leading to the

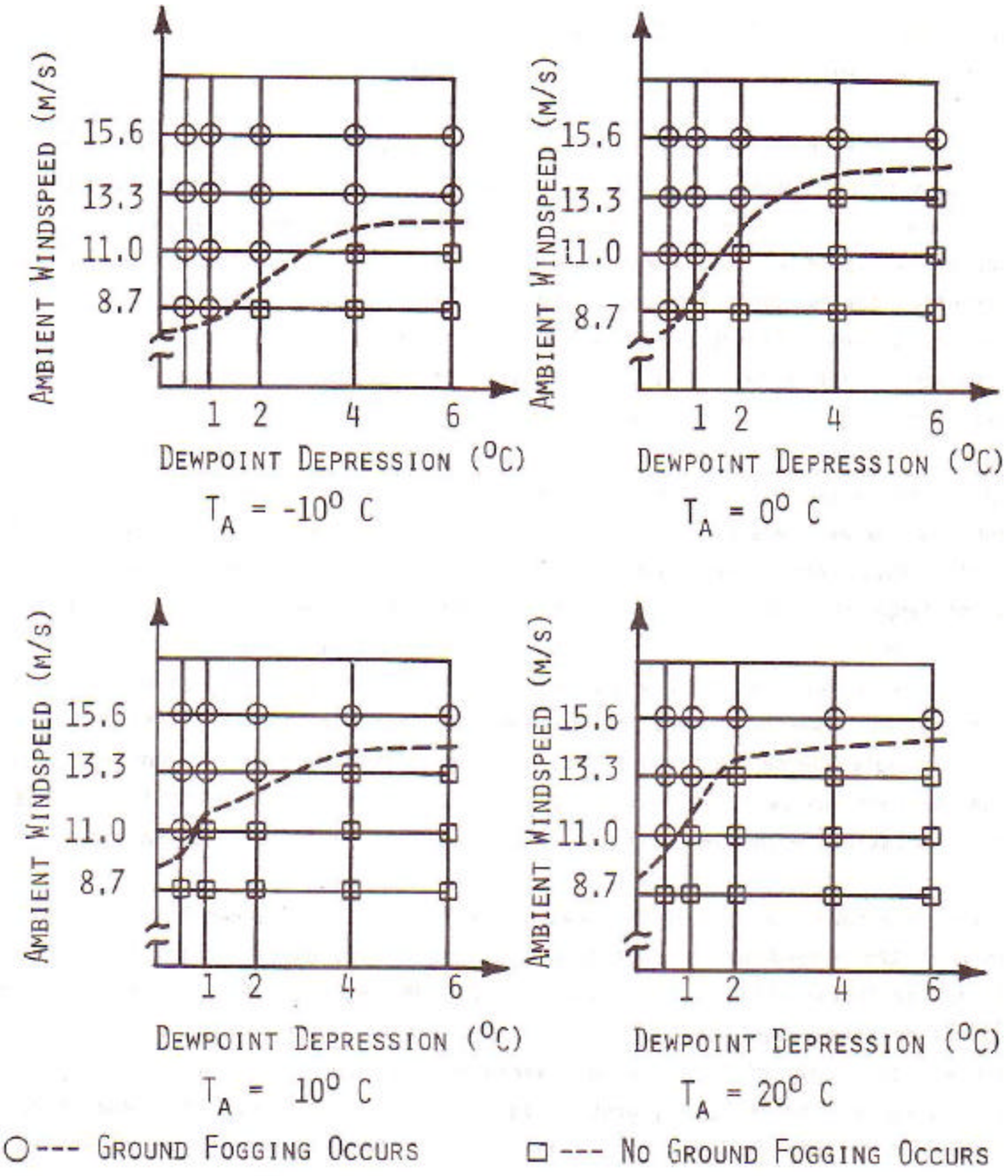

Figure 2-8. Calculation of the boundary between ground fog and no ground fog as a function of ambient wind speed, dew-point depression and ambient temperature for the standard LMDCT based on 80 test runs. The dotted lines show the approximate critical windspeed for occurrence of ground fog as a function of dew-point depression with the total heat dissipated by the tower (and the exit velocity) held constant.

most severe fogging predictions of the 80 runs. These ranges are shown in Table 2-1 for the CMDCT, and in Table 2-2 for the LMDCT. The values of input parameters for the single-source model for each of the ten fogging/icing cases are shown in Table 2-3. The first five cases which have average ambient temperatures below 0 deg. C, are assumed to contribute both to fogging and icing, while the last five, which have average ambient temperatures at or above 0 deg. C, contribute only to fogging.

At the time the site meteorological tape is being analyzed by the PREPROCESSOR, the number of hourly records contained in each fogging/icing category are accumulated; furthermore, representative cases were stored on disk for input to the plume model. If fogging and icing are computed at all, then all 10 category representative cases will be computed although not all fogging/icing categories may actually be represented in the meteorological data.

(a) fogging patterns

When a representative fogging/icing case is run with the PLUME Model, the model generates a ground fogging pattern in a manner which we now describe. In the model, the lesser of the plume temperature radius, R, and the visible radius, RV (determined from the Gaussian temperature and water distributions), is used in conjunction with the plume trajectory angle and the centerline height above the tower to check whether the "disk" of plume visibility at that distance from the tower would intersect the ground. Figure 2-9 illustrates the relevant geometry. For such a comparison we neglect ground interference effects on plume rise. The chord with which the ground surface intersects this disk is computed at each output step. These output steps are closely spaced within the first 1.6 km where we consider fogging to occur. At two successive steps where a nonzero chord is predicted, the chord ends are connected to form a trapezoid. This trapezoid is then distributed into the standard fogging subsectors bounded by the user-specified radii (or every 0.1 km out to 1.6 km if default value are used), and by rays separated 22.5 degrees apart. Thus, each subsector (bounded by two adjacent rays and two arcs of circles) will receive a fraction between 0 and 1 representing the fraction of the area of that subsector that is covered by the region of ground fog for the case being run. Fig. 2-10 shows one such trapezoid superimposed on the subsector pattern. Fig. 2-11 presents the fractional subsector values generated from category No. 1 for a CMDCT, along with an approximate outline of the fogging region.

Table 2-1. Category ranges for each of 10 standard cases of fogging/icing for a circular MDCT

CAT. NO. ---	RANGE IN TDB (deg. C)	RANGE IN U (m/sec)	RANGE IN DPD (deg. C)
1	< -5	12 - 15	0 - 1
2	< -5	> 15	0 - 1
3	< -5	12 - 15	1 - 3
4	< -5	> 15	1 - 3
5	< -5	> 15	3 - 6
6	-5 - 5	12 - 15	0 - 1
7	-5 - 5	> 15	0 - 1
8	-5 - 5	> 15	1 - 5
9	5 - 15	> 15	0 - 4
10	15 - 25	> 15	0 - 3

Table 2-2. Category ranges for each of 10 standard cases of fogging/icing for a linear MDCT

CAT. NO. ---	RANGE IN TDB (deg. C)	RANGE IN U (m/sec)	RANGE IN DPD (deg. C)
1	< -5	7.5 - 11	0 - 1
2	< -5	> 11	0 - 1
3	< -5	10 - 14	1 - 3
4	< -5	> 14	1 - 3
5	< -5	> 12.5	3 - 6
6	-5 - 5	> 9	0 - 1.5
7	-5 - 5	> 13.5	1.5 - 6
8	5 - 15	> 11	0 - 1.5
9	5 - 15	> 13.5	1.5 - 4
10	15 - 25	> 12.5	0 - 4

Table 2-3. Input parameters for 10 special cases selected on the basis of a CMDCT fogging study done to determine fogging categories

No.	WIND SPEED (m/s)	WIND SPEED EXPON.	TDB (C)	LAPSE (C/m)	TDP (C)	HT (m)	EXIT VEL. (m/s)	EXIT TEMP. (C)	LIQUID WATER (kg/kg)	MIXING HEIGHT (m)
001	13.5	0.25	-10.0	-.00975	-10.5	21.0	5.5	17.0	0.0	500.
002	17.5	0.25	-10.0	-.00975	-10.5	21.0	5.5	17.0	0.0	500.
003	13.5	0.25	-10.0	-.00975	-12.0	21.0	5.5	17.0	0.0	500.
004	17.5	0.25	-10.0	-.00975	-12.0	21.0	5.5	17.0	0.0	500.
005	17.5	0.25	-10.0	-.00975	-14.5	21.0	5.5	17.0	0.0	500.
006	13.5	0.25	0.0	-.00975	-0.5	21.0	5.5	22.0	0.0	500.
007	17.5	0.25	0.0	-.00975	-0.5	21.0	5.5	22.0	0.0	500.
008	17.5	0.25	0.0	-.00975	-3.5	21.0	5.5	22.0	0.0	500.
009	17.5	0.25	10.0	-.00975	8.0	21.0	5.5	27.0	0.0	500.
010	17.5	0.25	20.0	-.00975	18.5	21.0	5.5	33.0	0.0	500.

(Tower effective radius was 23.2 m).

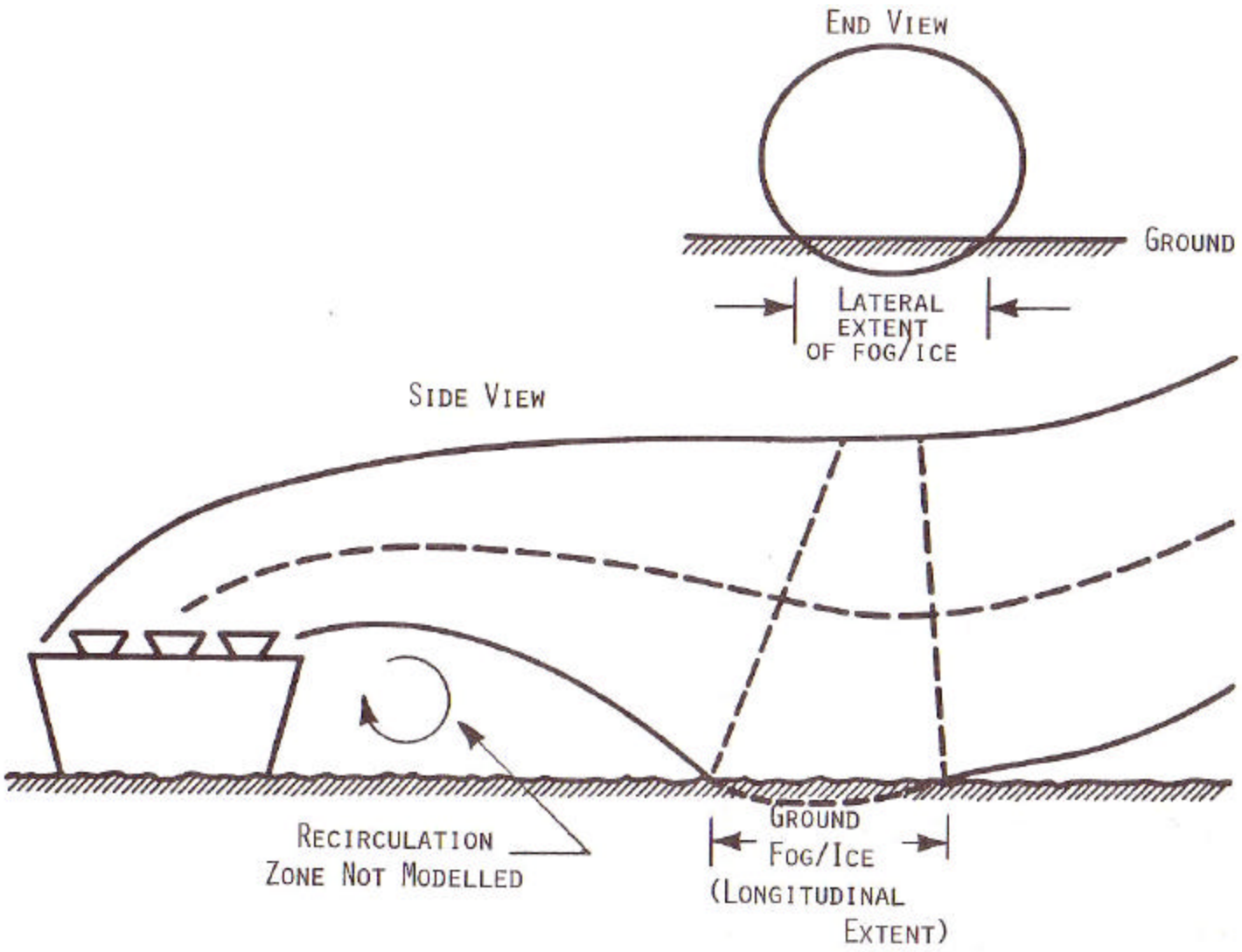

Figure 2-9. Relevant geometry for determining fogging/icing area of impact on ground.

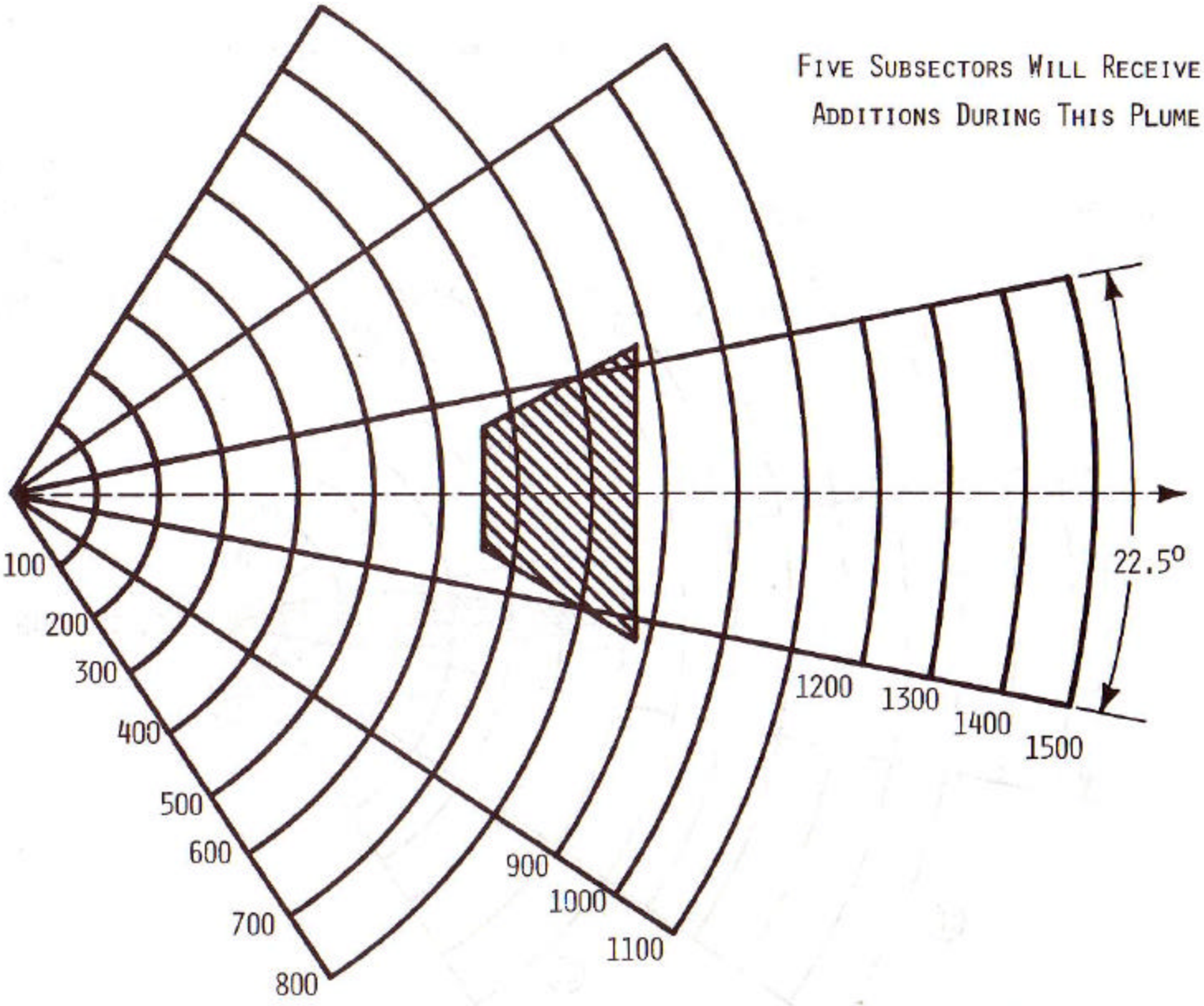

Figure 2-10. A trapezoid formed from chords at two output steps for fogging.

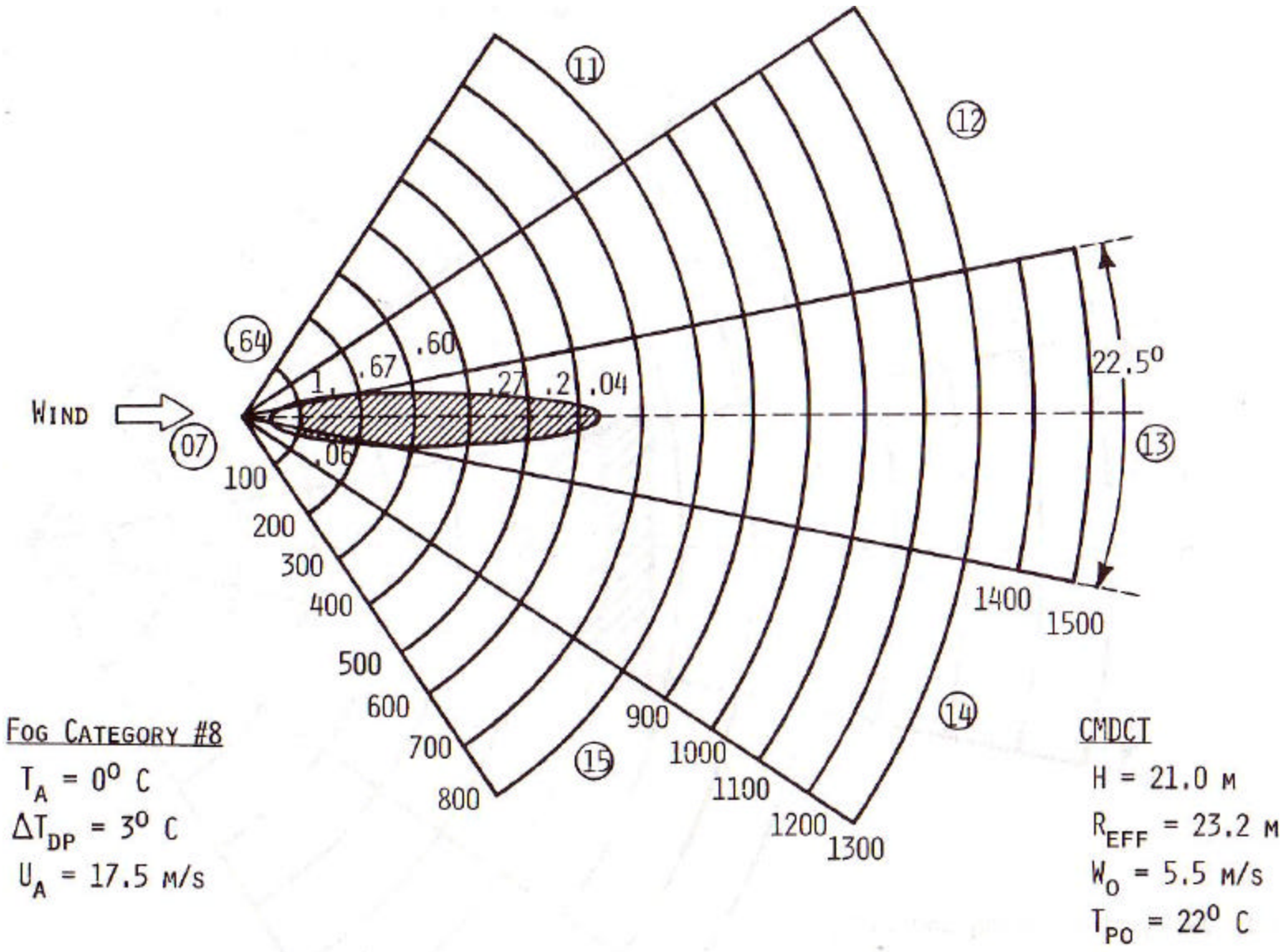

Figure 2-11. Fractional subsector values for category #1 with a CMDCT.

Further approximations are made for a LMDCT or for several LMDCTs or CMDCTs when fogging and icing are calculated using the multiple-source code for the representative case for each category. Only fogging/icing predicted for the (partially merged) main plume is tabulated. (This plume begins with the most upwind cell or port.) Furthermore, the resulting fogging/icing pattern is taken to be centered at the user-specified origin for the site. For a single LMDCT, where merging is rapid, this approximation is good. Also, for closely-spaced towers, the approximation seems reasonable.

(b) Seasonal/annual fogging and icing patterns

As the input meteorological data tape is being run by the PREPROCESSOR, the fogging/icing category number is added to each hourly record. The output of the PLUME Model runs contains 10 fogging patterns when IFOG = 1 is selected. In the TABLES code, these standard patterns are distributed with angle according to season and wind direction in the appropriate subsectors for all 16 angular sectors. Again, when PLUME is used, predictions are made for each standard wind direction for each of the 10 categories, and the results do strongly depend on wind direction. A frequency matrix, F(i,j,k), is accumulated from the hourly records where i is the category number (between 1 and 10), j is the season (between 1 and 5) and k is the wind direction (between 1 and 16). (Note that calm winds can never lead to fogging and never correspond to one of the categories.) Each matrix element is the number of hours that category i occurs in season j with wind direction k. A simple multiplicative sum for each season then produces a matrix of dimension 16 x NFRAD for hours of fog. The correlation between standard wind direction predictions and meteorological wind directions is done as before. This table is produced by TABLES as a hard copy and as a disk-file for use in plotting isopleths. If icing categories had nonzero frequencies of occurrence, a separate matrix is generated for icing using the frequency matrix elements for the first 5 (CMDCT) or the first 5 (LMDCT) categories. Isopleths for fogging and icing for an actual site will be presented in a later discussion of system outputs.

For a collection of CMDCTs (or LMDCTs) whose centers are spaced more than 2-3 tower diameters (or 2-3 tower longest dimensions) apart, the origin approximations mentioned above seem questionable for fogging and icing, which occur mainly in the near field. For these cases, if fogging/icing within 1.6 km of one of the towers would constitute a serious environmental impact, we recommend that the user rerun the PLUME code and the TABLES portion of the seasonal/annual system for a single

tower. Then the resulting seasonal/ annual fogging and icing patterns are assumed to occur once for each tower, centered at that tower; and the resulting (probably overlapping) patterns are combined to produce a single cumulative pattern centered at the user-specified origin. Clearly, in the overall subsectors where individual tower patterns overlap, multiple counting of fogging/icing hours will result, but the predictions then become conservative, which is acceptable. Most importantly, a more detailed near-field representation of fogging and icing with tower geometry will result. We have written a simple code to access the relevant tables on the TABLES output disk file and then perform this combination (COMBINE).

Plume Shadowing

Since the methodology for calculating several seasonal/annual measures of shadowing has been described previously in Carhart, Policastro and Dunn (20), a detailed discussion is not necessary here. In the above reference, methods are outlined and our methodology is described. A brief outline, then, is given below with an emphasis on the one major change employed in our methodology: the schematization of the plume shape for each hourly record.

There are four basic measures of plume shadowing which can be presented within a seasonal/annual scheme. They are as follows:

(1) Hours of shadow at a given point on the ground.
(2) Energy loss at a point on the ground in megajoules per square meter, (mj/m^2).
(3) Percentage loss of total solar energy reaching the ground.
(4) Percentage loss of direct (beam) solar energy reaching the ground.

If a beach or recreational area might be impacted by the plumes from a tower installation, then hours of shadow might be the most useful measure to consider. If shadowing of nearby croplands were at issue, then fractional loss of total solar energy would probably be most important, and would be especially useful if the growing season were selected as one of the five seasons. However, if the environmental impact issue centered around loss of solar energy deposited in a focusing solar collector adjacent to the plant, then fractional loss of beam solar energy would be appropriate. If monetary compensation for lost solar energy were under consideration for some location near the tower but outside the actual plant site, loss of solar energy per square meter would be the needed information.

Because it is difficult to anticipate the kinds of environmental impact issues which may arise involving shadowing during the next few years, we have elected to set up our seasonal/annual system to generate all four types of shadowing information.

Our seasonal/annual methodology leads to the designation of a category number for each hourly record. Since we know which category a given hourly record is represented by, this leads us to assign a plume length, L, a plume height, H, and a plume final temperature radius, R, computed with the PLUME Model for the category representative conditions. We use a simplified model geometry for the plume shadow for each hourly record, based on the L, H and R values, and accumulate the shadows from each hour. In this way the actual hourly sun angles can be used, and correlations between plume size and time of day can be fully represented. We believe this is the most important correlation we need to include to model shadowing accurately because, for example, long plumes frequently occur during the early daylight hours, while late afternoon plumes are generally shorter. Correlations between plume size and season are accommodated in this method also, as they would be in some other methods. We have thus chosen not to use a frequency matrix approach for calculating shadowing, (i.e., choosing 35 representative shadowing cases as we did for plumes and drift), although we could have provided very accurate shadow patterns for each of the detailed category-representative cases. Such a method cannot reflect hourly and seasonal shifts in shadow location for a given predicted plume shape.

For the purposes of determining the plume shadow outline on the ground for a given hourly record, the actual predicted plume for the hourly category representative was idealized in our previous study as a cylinder of radius 0.7 times the final temperature radius, of length equal to the visible plume length, and of height equal to the tower height plus 0.5 times the visible plume rise above the tower. Neglecting end effects, this cylinder would cast a parallelogram shadow on the ground whose actual location was determined from the wind direction (which gave the orientation of the cylinder) and the solar altitude and azimuth angles. This idealized parallelogram shadow was then distributed into the relevant standard subsectors defined by the 16 angular sectors and 50 circles spaced 0.2 km radially, stored in the program as a 16 by 50 array for each season. Two such arrays were kept, one for hours of shadow and the other for the solar energy deposition loss in megajoules per square meter (mj/m^2). The resulting hours of shadow and amount of solar energy loss contributions in each subsector were summed for every daylight hourly record in the season. These matrices were then easily used to produce isopleths of each of the four measures of shadowing listed above.

To predict the average hourly direct (beam) and diffuse components of the solar flux at ground level from data contained in commonly-available weather tapes is well beyond the present state-of-the-art. However, in solar energy design work, considerable progress has been made in predicting reliable average daily solar energy fluxes, and even long-term average hourly values of direct and diffuse solar energy flux, as described in Collares-Pereira and Rabl (21) and Liu and Jordan (22). Required for a site are the latitude and longitude, the monthly clearness indices, K(i), and the average daily total solar flux on a horizontal surface at sea level for each month, H(i). As a result of the SOLMET program (23), monthly values of K and H are available at about 260 sites across the continental United States, Canada, Alaska and Hawaii. (These values vary smoothly from one site to the next in many parts of the country, which would allow interpolation for most locations.) These values are given in Appendix B, along with a map of the available locations.

Finally, in determining the amount of loss of solar energy in the shadow (the "darkness" of the shadow), it was necessary to approximate the absorption of the direct component of the solar flux as it passes through the plume. Although this value varies from the "center" of the shadow, where it is greatest, to zero at the edge, it was decided to assume that the absorption at the thickest point would be used for the whole shadow. This simplification makes the calculations much less costly, and produces clearly conservative results. Because no reliable values of plume liquid water content and cloudwater droplet spectrum can be predicted at present, it was decided to assume a standard optical density for the visible plume, with an absorption length fitted to a plume shadow measured in the field; (for details, see Ref. (20)). The fraction of direct solar flux was taken to be

$$f = 1 - \exp(-0.0165*D).$$

where D is the plume final temperature diameter in meters.

In the multiple-source model, the principles described above are all followed, but the idealized plume shape is made somewhat more realistic. We now assume that the visible plume is approximated by the section of a cone cut off by two planes perpendicular to the axis so that the smaller face has as its radius the tower exit radius for single sources, and the larger face has as its radius the final temperature radius of the visible plume. This shape overestimates the extent of the actual predicted visible plume, again yielding conservative shadowing results. This truncated cone is assumed to lie at an upward-slanting angle from the tower

outlet to the location of the centerline where the visible plume disappears. Fig. 2-12 illustrates this idealized shape for a hypothetical visible plume. Again neglecting end effects, the shadow of such an object on the ground is a quadrilateral, which is then distributed into the appropriate subsectors in the same way as was the previous parallelogram shadow. Of course, a given subsector will receive only a fraction of an hour or a fraction of the solar energy loss if the shadow covers only a part of that subsector. Fig. 2-13 illustrates one of these quadrilateral shadows superimposed on the subsector pattern, with approximate filling fractions listed.

When a multiple tower or multiple cell (e.g., one LMDCT) case is being run, predictions of the PLUME code are available to the TABLES code (where shadowing data are actually accumulated). A run is made for each category representative case. In such a situation, only one change in the above procedures is made from the equivalent source plume case. Instead of using the source exit radius as the initial radius of the section of the cone, as shown in Fig. 2-9, an initial radius is computed for each hourly record as the minimum of one cell radius and one-half the maximum crosswind distance between any pair of cell centers. (If the user sets the variable RSTAR to a nonzero value, then this value overrides the calculation of this crosswind extent of the installation for all hourly records.) Such a procedure generally gives an initial plume extent that is too large; in particular, it yields a continuous visible plume across the entire installation even before merging has occurred. It will strongly overpredict near-field shadowing.

Near-field shadowing occurring within plant boundaries is normally not of critical concern. However, in one application, a plant-operated greenhouse was being studied to utilize reject heat. In this case, a more realistic near-field shadowing calculation might be desired, although the very conservative method described above may still predict acceptable shadowing levels.

To circumvent near-field shadowing overprediction, the user has two choices:

(a) a reasonable value of RSTAR may be given to limit the initial cone radius to the size of a single tower, for example, or
(b) more realistically, the user could rerun PLUME for a single tower. The resulting predictions could then be used in TABLES, with the needed shadowing tables merged together using the COMBINE code, as described for fogging and icing calculations above.

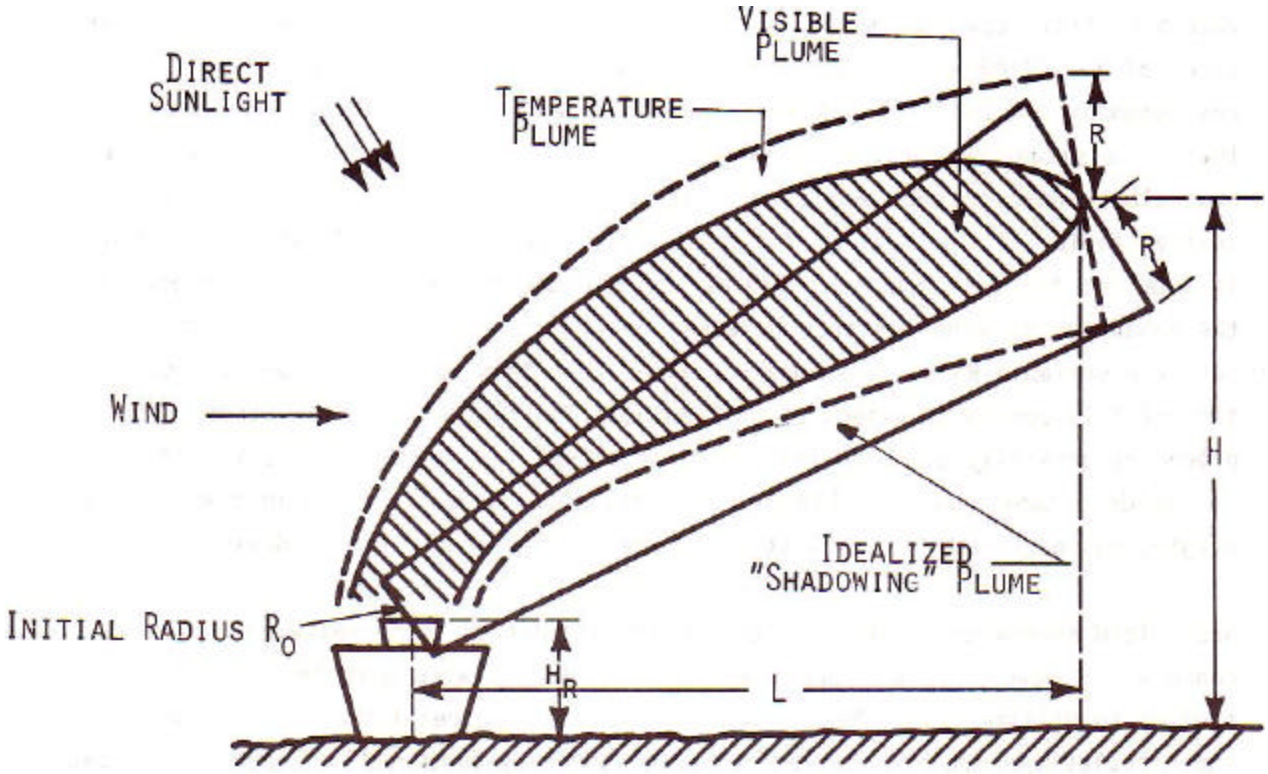

Figure 2-12. Method of representation of plume of shadowing submodel.

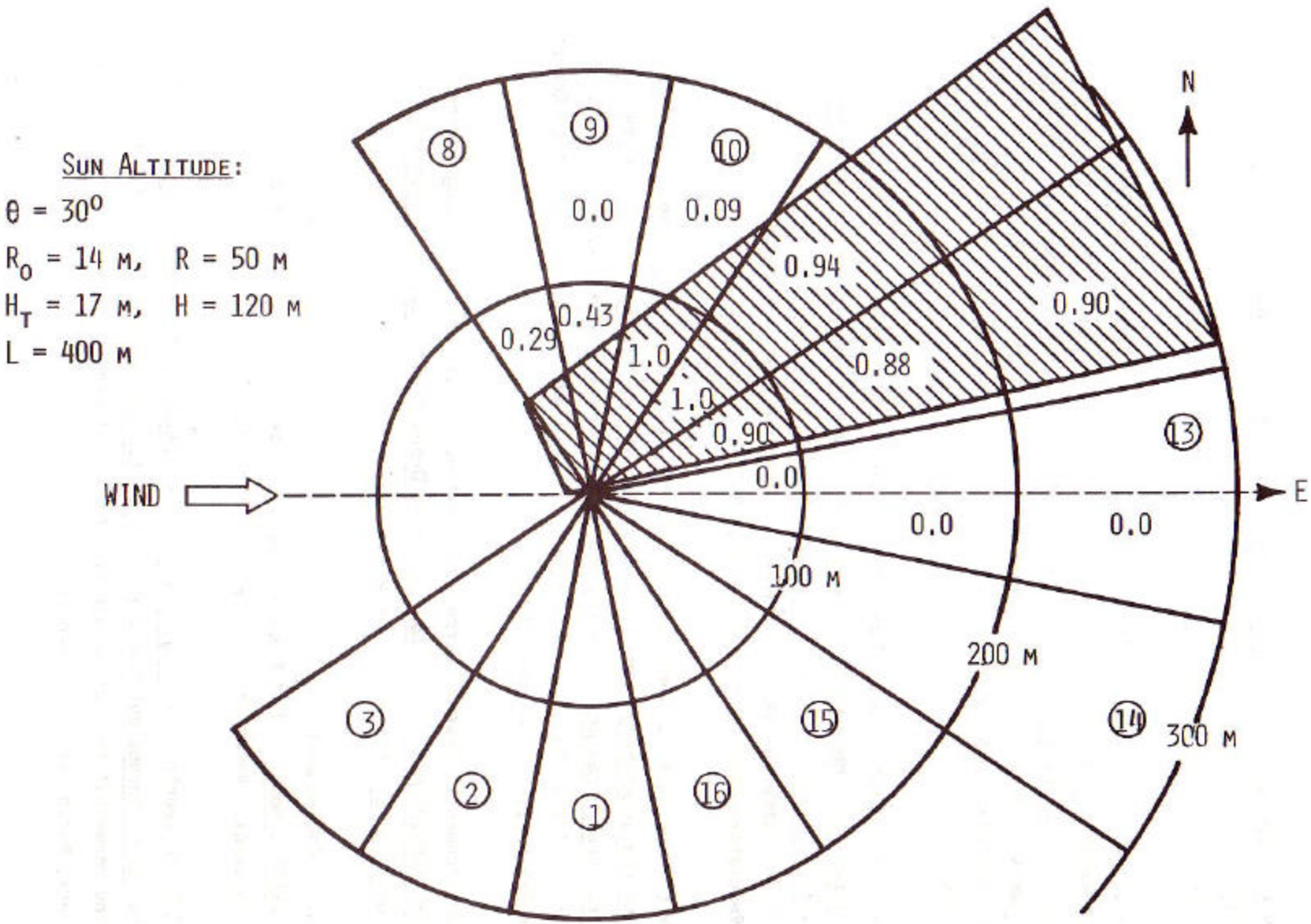

Figure 2-13. Sample shadow on polar coordinate grid system.

REFERENCES

1. M.E. LaVerne. Oak Ridge Fog and Drift Program (ORFAD) User's Manual. Oak Ridge National Laboratory, Report No. ORNL/TM-5021. Oak Ridge, Tennessee 1976.

2. A.J. Policastro, R.A. Carhart, S.E. Ziemer, K. Haake. Evaluation of Mathematical Models for Characterizing Plume Behavior from Cooling Towers. Vol. 1. Dispersion from Single and Multiple Source Natural Draft Cooling Towers. Division of Environmental Impact Studies. Argonne National Laboratory. U.S. Nuclear Regulatory Commission Report NUREG/CR-1581. June 1979.

3. A.J. Policastro, W.E. Dunn, M.L. Breig, J.P. Ziebarth. Evaluation of Mathematical Models for Characterizing Plume Behavior from Cooling Towers. Vol. 2. Salt Drift Deposition from Natural Draft Cooling Towers. Division of Environmental Impact Studies. Argonne National Laboratory. U.S. Nuclear Regulatory Commission Report NUREG/CR-1581. February 1979.

4. W.E. Dunn, G.K. Cooper, and P.M. Gavin. Evaluation of Mathematical Models for Characterizing Plume Behavior from Cooling Towers. Vol. 3. Plume Rise from Mechanical Draft Cooling Towers. Department of Mechanical Engineering, University of Illinois at Urbana. U.S. Nuclear Regulatory Commission Report NUREG/CR-1581. December 1979.

5. Environmental Systems Corporation and Motor Columbus Consulting Engineers. The KUMULUS Model for Plume and Drift Deposition Calculations for Indian Point No. 2. Knoxville, Tennessee 1977.

6. U.S. Environmental Protection Agency. User's Manual for Single-Source (CRSTER) Model. EPA-450/2-77-013. Office of Air Quality Planning and Standards. Research Triangle Park, North Carolina. July 1977.

7. G.C. Holzworth. Mixing Heights, Wind Speeds, and Potential for Urban Air Pollution Throughout the Contiguous United States. Division of Meteorology. Environmental Protection Agency. Office of Air Programs. Research Triangle Park, North Carolina. January 1972.

8. A.J. Policastro, W. Dunn, and R. Carhart. Studies on Mathematical Models for Characterizing Plume and Drift Behavior from Cooling Towers. Executive Summary. Report No. EPRI CS-1683. April 1981.

9. A.J. Policastro and M. Wastag. Studies on Mathematical Models for Characterizing Plume and Drift Behavior from Cooling Towers. Volume 1. Mathematical Model for Single-Source (Single-Tower) Cooling Tower Plume Dispersion. Report No. EPRI CS-1683. Volume 1. January 1981.

10. R.A. Carhart, A.J. Policastro, S. Ziemer, K. Haake, and W. Dunn. Studies on Mathematical Models for Characterizing Plume and Drift Behavior from Cooling Towers. Volume 2. Mathematical Model for Single-Source (Single-Tower) Cooling Tower Plume Dispersion. Report No. EPRI CS-1683. Volume 2. January 1981.

11. W.E. Dunn, P. Gavin, B. Boughton, A.J. Policastro, and J. Ziebarth. Studies on Mathematical Models for Characterizing Plume and Drift Behavior from Cooling Towers. Volume 3. Mathematical Models for Single-Source (Single-Tower) Cooling Tower Drift Dispersion. Report No. EPRI CS-1683. Volume 3. January 1981.

12. A.J. Policastro, R.A. Carhart, and M. Wastag. Studies on Mathematical Models for Characterizint Plume and Drift Behavior from Cooling Towers. Volume 4. Mathematical Model for Multiple-Source (Multiple-Tower) Cooling Tower Plume Dispersion. Report No. EPRI CS-1683. Volume 4. January 1981.

13. A.J. Policastro, W.E. Dunn, M. Breig, and K. Haake. Studies on Mathematical Models for Characterizing Plume and Drift Behavior from Cooling Towers. Volume 5. Mathematical Model for Multiple-Source (Multiple-Tower) Cooling Tower Drift Dispersion. Report No. EPRI CS-1683. Volume 5. January 1981.

14. A.J. Policastro, M. Wastag, W.E. Dunn, and R. Carhart. Validation of Cooling Tower Plume Model at the Philippsburg and Geysers Sites. Presented and Published at International Association of Hydraulic Research Cooling Tower Workshop. Budapest, Hungary. October 12-15, 1982.

15. F.H. Wu and R.C. Koh. Mathematical Models for Multiple Cooling Tower Plumes. W.M. Keck Laboratory for Hydraulics and Water Resources. Report KH-R-37. California Institute of Technology. July 1977.

16. E. Ryznar, D. Baker, M. Weber, D. Kalibaum, and M. St. Peter. An Investigation of the Meteorological Impact of Mechanical Draft Cooling Towers at the Palisades Nuclear Plant. Department of Atmospheric and Ocean Science. University of Michigan. January 1980.

17. W. Caspar and W. Scharrer. Measurements of the Atmospheric Conditions and Observations of the Cooling Tower Plume. IN: Studies on a Natural Draft Wet Cooling Tower. VDI Report. Vol. 15. No. 5. Ed. G. Ernst. pp 57-69. July, 1974.

18. J. Vogel. Personal Communication. Illinois State Water Survey. Champaign, Illinois. 1979.

19. P.R. Slawson, T.L. Crawford, C.H. Goodman, and E.R. Champion. Observations of the Mechanical-Draft Cooling Tower Plumes at Plant Gaston (Data Report). Environmental Fluid Mechanics Group, Department of Mechanical Engineering, University of Waterloo; and Southern Company Services Inc. Birmingham, Alabama. February 1979.

20. R.A. Carhart, A.J. Policastro, and W.E. Dunn. An Improved Method for Predicting Seasonal and Annual Shadowing from Cooling Tower Plumes. Presented and Published in Proceedings of Third Conference on Waste Heat Management and Utilization. Miami Beach. May 1981.

21. M. Collares-Periera and A. Rabl. The Average Distribution of Solar Radiation - Correlations Between Diffuse and Hemispherical and Between Daily and Hourly Insolation Values. Solar Energy. Volume 22. pp. 156-164. 1979.

22. B.H.Y. Liu and R.C. Jordan. The Interrelationships and Characteristic Distribution of Direct, Diffuse and Total Solar Radiation. Solar Energy. Volume 4. p. 1. 1969.

23. SOLMET Manual. Volume 2. (Available from the National Climatic Center. Asheville, North Carolina.) 1978.

Appendix D

GUIDELINES FOR PLUME PREDICTION IN COMPLEX TERRAIN

INTRODUCTION

The EPRI system of codes for calculating seasonal/annual cooling tower environmental impacts assumes that the surrounding terrain is level and has uniform ground cover. On the other hand, one can encounter terrain which is very uneven and complex with strong vertical relief. In very complex terrain, the EPRI plume model would need to be modified to predict a detailed wind field along with the feedback that wind field would have on the plume and drift predictions. Between these two extremes, the user is often faced with certain relatively simple types of complex terrain, such as a ridge or a hill or a change in ground cover. In these cases enough is known about flow modification under various meteorological conditions to allow us to apply simple procedures for modifying certain of the output tables which show the seasonal or annual impacts. Thus, the usefulness of the ANL seasonal/annual system can be extended to include many frequently met cases of mild complex terrain.

In this Appendix, we describe the basic physics of airflow and plume behavior for five ideal types of complex terrain. We also recommend procedures for modifying the tables for plume length and for salt deposition to account for each terrain type. Our study of the five ideal terrain types using common meteorological conditions suggests that the flat, uniform terrain results usually provide a good approximation. As a result, suggested changes to table entries are small. If the user has a difficult case involving complex terrain which contains several categories of complex terrain or which does not fit the category scheme presented here, and if the environmental impact of the plumes is especially critical for such a site, he should obtain a model specifically developed for flow and dispersion over complex terrain, such as that developed by Yocke and Liu at Systems Applications Inc., San Rafael, CA (1). It is planned at SAI to modify their model to specifically handle cooling tower releases.

Plume behavior in complex terrain differs from that of the identical problem in flat terrain in a variety of ways. The plume can go around or over ridges and

hills depending on plume height, wind speed and stability. In complex terrain, atmospheric turbulence is often heightened causing plumes to disperse faster (become shorter) and drift to be deposited closer to the tower. Differences in vertical wind profiles between flat and complex terrain cause longer or shorter plumes, and change the downwind distances at which drift is deposited. The plumes may follow the terrain or maintain a constant elevation (after the rising phase) depending on stability, details of terrain types, and wind speed.

Apart from terrain geometry, the most important variables in the problem are:

1. atmospheric stability
2. wind speed at plume height
3. plume final height with respect to the surrounding terrain.

We shall assume that by the time the plume is significantly affected by terrain features, it can be considered as a passive tracer in the surrounding air flow. Consistent with this assumption, we will only consider the effects of terrain features that are more than 1.5km from the tower cluster.

Among the important parameters that could be incorporated into the plume model to account for terrain influences are corrections to plume height, length, diffusion coefficient, drift deposition, and shadowing. For environmental impact evaluations, plume length and drift deposition are usually the most important impacts to be predicted and handling the changes to these tables caused by complex terrain is more straightforward than for the other effects. Therefore, we chose to develop methods that modify only our frequency tables of plume length and salt deposition in order to account for terrain influences.

In considering modifications to the TABLES code output (plume length and drift deposition), it should be kept in mind that the air flow around terrain features is highly complex and is still the subject of intensive research. A considerable amount of engineering judgment must be exercised for each case. Because we wanted to develop sufficiently general and useful rules of thumb, we had to restrict ourselves to a first approximation in the modification of our predicted results. On the other hand, there is enough physical information about each case in this report and in the references cited to enable the user to modify the output in more detail if he wishes.

We shall consider here the following ideal types of complex terrain:

1. a change in surface roughness
2. hilly terrain
3. uniformly sloping terrain
4. a two-dimensional isolated ridge
5. a three-dimensional isolated hill.

In each case the basic plume behavior will be discussed, then rules of thumb for the TABLES code output modification will be established and some illustrative examples given.

Classification of Actual Terrain into the Five Idealized Types

First we consider important factors concerning terrain features of types 2 through 5. For example, a change in the roughness of the surface should not be considered as a change in terrain geometry. We define a significant terrain feature as any change in elevation that is an order of magnitude greater than the average roughness length of the terrain surface, and which is at least 10m. Figure D-1 shows an example of uniformly sloping terrain. This example is characterized by no changes in elevation greater than 10m and surface roughness assumed to be 1.5m (typical of a residential area). These elevation changes would have to exceed 15m to cause the terrain to fail to qualify as uniformly sloping.

At this point, we can briefly characterize the five terrain types which will be discussed in detail in the corresponding sections. First, let us consider basically flat terrain which has a change in the surface roughness height. The surface roughness height for a variety of ground covers has been studied extensively in an attempt to characterize flow in the planetary boundary layer. The ground cover changes from place to place over most terrain, and so does the effective roughness height. (The roughness height is usually much less than the physical height of the ground cover.) For example, sections of wooded ground may alternate between regions of grassy field, meadow or buildings. An idealized boundary can usually be drawn between two regions of different surface roughness. We imagine the surface roughness to stay constant over each region, but to change abruptly at the idealized boundary. The treatment of a change in surface roughness length is straightforward. A change in L by less than a factor of 5 can be ignored.

A second ideal type of terrain is hilly terrain. Hilly terrain refers to a region where the average elevation of the ground is not changing, but an irregular or

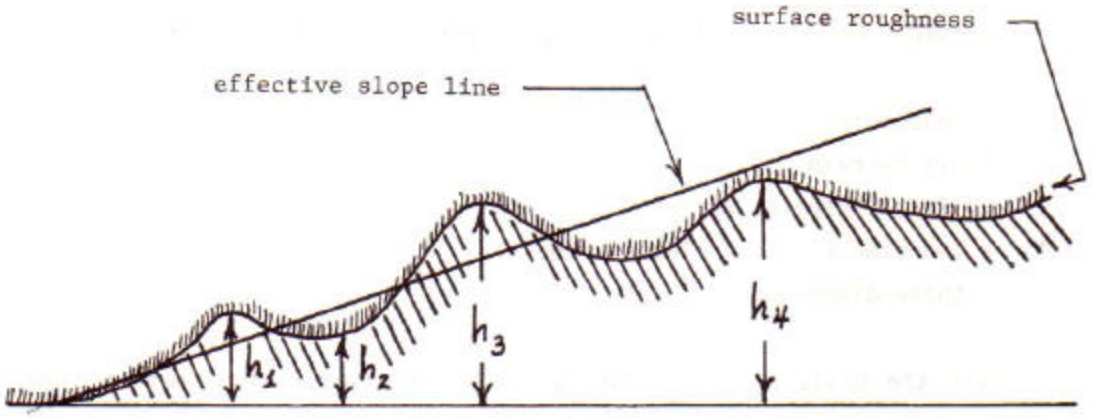

$h_1 = 5m$; $h_2 = 3.5m$; $h_3 = 12m$; $h_4 = 13m$

$h_2 - h_1$, $h_3 - h_2$, $h_4 - h_3$, etc. are all smaller than 10 L (15 m), where L is the surface roughness length.

Figure D-1. An example of undulating terrain which is classified as uniformly sloping terrain.

regular collection of moderately-sized hills occupy the region. If no hill has a slope exceeding 5%, the terrain is considered to be flat. Further, plume behavior will not be significantly modified unless the average hill height is more than about 50m.

When we encounter uniformly-sloping terrain as characterized above, either the centerline of one angular sector is essentially oriented along the direction of steepest slope, or a boundary between two adjacent sectors is so oriented. Next-nearest sectors then contain sloping terrain with a smaller slope. Thus, we must treat the TABLES code output modifications as a function of (sector) angle with respect to the direction of steepest ascent or descent. The maximum slope we recommend for identifying this type of terrain is that of a 30° angle (0.57); the minimum slope is that of a 5° angle.

The next ideal terrain type we describe is a two-dimensional ridge. The terrain will contain a ridge if there is a region of elevated ground which is much longer in one dimension than along a perpendicular dimension. The cross section of the ridge (considered perpendicular to the long axis) should be approximately constant

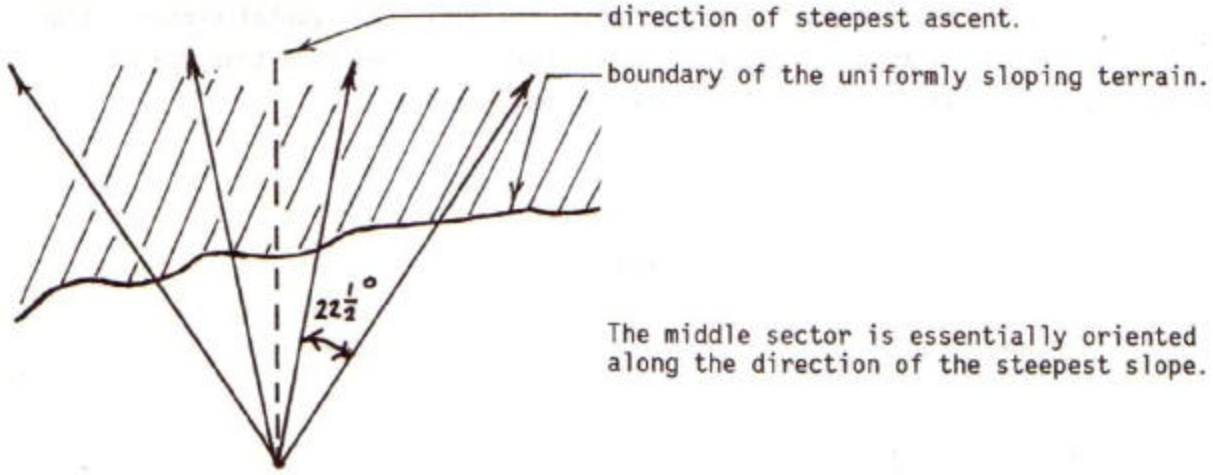

Figure D-2. A possible angular orientation of uniformly sloping terrain with respect to the wind direction sectors.

The ends of the ridge should subtend an angle of at least 67½° (3 sectors) at the tower cluster; otherwise, it can be treated as an isolated hill. If the elevation of the ridge is less than 50m or if the ridge is more than 3.5km from the tower cluster, no important consequences are likely to occur. The most significant effects of ridges occur when they rise more than 100m and they lie within 2-3km of the tower. Two examples of a ridge are shown in Fig. D-3.

In Fig. D-3(a), the ridge subtends the three sectors completely, but in Fig. D-3(b) sectors 3 and 16 are only partially subtended. The first case is handled straightforwardly as discussed below; the second case needs some clarification. In sectors 3 and 16, the ends of the ridge can be viewed as a semi-hill. Thus, after treating the effects in sectors 1 and 2 as for a normal ridge, the effects in sectors 16 and 3 can be adjusted using hill formulas by moving deposition rates to one side only.

Finally, we will characterize a <u>three-dimensional (3D) hill</u>. A hill is an isolated elevation of the ground surface, which can occur in a variety of shapes. (Minor double-peaking or small elevated valleys can be ignored.) As distinguished from a

"finite-length" ridge, a hill subtends fewer than three full sectors (67½°) at the tower cluster. To produce significant effects, the hill's horizontal cross-section at an elevation 200m above the tower cluster should subtend more than 2/3 of a sector (15°). (A hill less than 200m high can be ignored).

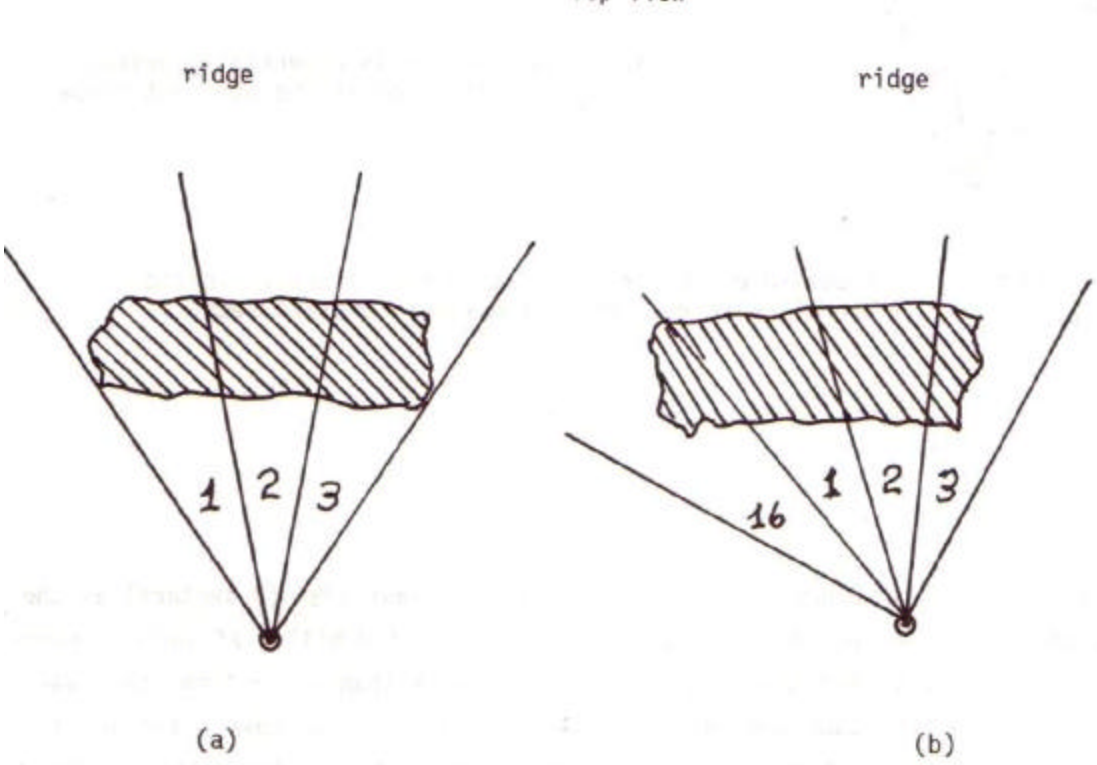

Figure D-3. Illustrations of the definition of a two-dimensional ridge.

In summary, the first step the user must take in considering complex terrain effects is to analyze a local topographic map which also shows ground cover, and apply the above criteria to establish the occurrence of one or more ideal terrain types. Clearly, overlapping terrain types, such as a 3D hill on which ground cover changes, cannot be fully analyzed by these methods.

In the following five sections, we will first describe qualitatively the behavior of a single plume as it is affected by each of the five ideal terrain types. Then we will present a set of rules for modifying two of the seasonal/annual tables

produced by the TABLES code (the plume length frequency table and the salt drift deposition table) for each season in the presence of the terrain feature.

In order to make these modifications, three special tables are also produced in our TABLES program output for each season and printed. These are:

(1) a frequency table for the seven Pasquill stability classes as a function of wind direction. (We consider classes 1-3 as unstable, 4 and 5 as neutral, and 6 and 7 as stable.)
(2) a frequency table for three wind-speed ranges (taken at 200m above tower elevation) by wind direction. These ranges are:
    (a) low (0-3)m/s
    (b) moderate (3-7)m/s
    (c) high (>7)m/s
(3) a joint frequency table combining 1) and 2), by wind direction.

The general simplifying assumptions we have used for plume and drift behavior in the prescriptions below are the following:

(1) By the time the plume is significantly affected by the terrain feature, it can be treated as a passive tracer in the surrounding air flow. To assume this, we require that the terrain feature be located at least 1.5km from the center of the tower cluster.
(2) A standard 50m interval is used for the radial extent of all subsectors. (The user can modify the formulas for other interval choices.)
(3) The drift droplets follow the centerline, disperse laterally in a Gaussian distribution, and the heavier droplets have fallen to the ground closer than 1.5km to the origin. (This assumption seems valid from numerical studies of droplet trajectories and enables one to treat the remaining lighter droplets as passive tracers.)

To illustrate the general method of using the stability class and wind speed range tables, we consider a subsector entry A_{ij} in one of the tables for modification (plume length frequency or salt deposition rate), where i refers to the radial location and j to the wind direction (sector number, 1-16).

(1) Suppose the value A_{ij} is to be moved to subsector (k,l) <u>if</u> the ambient stratification is <u>stable</u>. The two stable Pasquill classes are F and G (6 and 7). Thus, if f_{ij} represents the frequency-of-occurrence entry in the i^{th} class and j^{th}

wind direction of the stability-class frequency table, we would add to subsector A_{kl} only the amount

$$(f_{6j} + f_{7j})\, A_{ij},$$

and leave the remaining amount in subsector (i,j).

(2) If the removal of A_{ij} to subsector (k,l) depended upon both ambient stability and low-to-moderate winds, and if the value g_{mj}, $(1 \leqq m \leqq 3)$, is in row m and column j of the wind-speed range frequency table, then the fraction of A_{ij} to be removed from (i,j) to (k,l) would be:

$$(f_{6j} + f_{7j})\, (g_{1j} + g_{2j})\, A_{ij},$$

with the remainder left in subsector (i,j).

The third special table produced for each season in the TABLES code provides these joint-frequency products including the indicated summations. (See Table D-4).

A Change in Surface Roughness (2)-(5).

Over most natural terrain, surface roughness is not homogeneous but changes significantly from location to location. For instance, patches of wooded area alternate with patches of fields or meadows. A useful table of surface roughness heights is given in Ref. (2), and is reproduced below as Table D-1.

An idealized boundary can usually be drawn between two regions of different surface roughness at which the surface roughness changes discontinuously. The boundaries between regions must be established from a map of the site showing not only elevation but ground cover and man-made structures.

To estimate the order of magnitude of effects for a variety of sites for annual or seasonal averages, we assume neutral atmospheric stratification on the average. We also assume average plume leveling heights of 200m (beyond 1.5km from the tower) for MDCT plumes and 300m for NDCT plumes.

The transition region for reestablishment of the planetary boundary layer is about 1 km (2) so that by the time the influence of the roughness change reaches a

Table D-1. Surface roughnesses for various ground covers.

Type of Surface	Z_o[cm]	Indentifier
Mud flats, ice	10^{-3} - $3 \cdot 10^{-3}$	MFI
Smooth sea	$2 \cdot 10^{-2}$ - $3 \cdot 10^{-2}$	WA
Sand	10^{-2} - 10^{-1}	SD
Plain, snow covered	0.49	SP
Grassy surface	1.73	GS
Mown grass	10^{-1} - 1.0	MG
Low grass, steppe	3.2	LG
Flat country	2.14	FC
High grass	3.94	HG
Wheat	4.5	WH
Beets	6.4	BE
Palmetto	10 - 30	PL
Low woods	5 - 10	LW
High woods	20 - 90	HW
Suburbia	100 - 200	S
City	100 - 400	C

height of 200 m, it will be at least 1km beyond the boundary. This places the earliest effects at about 2.5km away from the tower cluster. Starting from that point, plumes from a rough-smooth transition will move faster and will generally become longer. Tables of plume length frequencies and salt deposition have to be modified correspondingly. (The frequency of long plumes beyond 2.5km should increase and salt deposition should occur further from the towers.) Of course, for a smooth-rough transition, the picture is reversed (plumes become shorter and drift is deposited closer to the towers).

We now suggest simple formulas for TABLES output modification. Consider a rough-smooth transition. Define $m = \frac{(\text{surface roughness})_1}{(\text{surface roughness})}$. Clearly $m > 1$ for a rough-smooth transition. For example, from Table D-1 for a (low woods) → (low grass) transition, $m \cong \frac{7.4\text{cm}}{3.2\text{cm}} \cong 2$.

As was said above, the transition region is about 1km in radial extent. There are no data available for the far downstream region (2), but near the boundary the change in the wind speed can be approximated by the following formula:

1. for $m < 1.5$ $\quad u' \cong u$
2. for $m > 1.5$ $\quad u' \cong u\,(1 + 0.0036m)$

Here u is the initial wind speed and u' is the corrected one.
For m=5 (as in a woods-grass transition), u' = 1.015u; for m=100 [high woods → low grass], u' = 1.3 u. With this information, we can specify an approximate method for modifying the length and drift tables because knowledge of the new wind profiles enables us to estimate changes in plume lengths and in the distances at which drift droplets are deposited.

Rough-Smooth Transition.

(1) Plume Length Frequency Table.

(a) Draw the boundary between areas of differing roughness and wind direction sectors on a copy of the topographical map. Determine at which radial subsector the transition occurs in each sector which includes it.

(b) Compute $m = \frac{\text{(surface roughness length of tower area terrain)}}{\text{(surface roughness length of new terrain)}}$. The remaining steps are to be done for each wind direction sector which includes the boundary.

(c) If $m < 1.5$, make no modifications. If $m > 1.5$, leave the first four subsectors (200m) beyond the boundary unchanged. Then increase the frequency values in each of the more remote subsectors according to the formula

$$f' = f\,[1 + 0.0036m]$$

(d) If there are zero frequencies in subsectors far from the origin, extend the last nonzero value which occurs at distance L_{max} from the towers to a new maximum distance of

$$L'_{max} = L_{max}\,[1 + 0.0036m]$$

adjusted to the nearest subsector boundary.

(2) Salt Drift Deposition Table.

To modify the salt deposition rate table, carry out steps 1(a)-1(d) again, where f' and f now represent salt deposition in kg/(km^2-month).

(Although this procedure results in slightly more total salt deposition than the unmodified table does, it is a conservative estimate of the environmental impact of the drift.)

Smooth-Rough Transition.

(1) Plume Length Frequency Table.

(a) After drawing the boundary and the wind direction sectors on a copy of the topographical map of the area,

$$\text{compute } m = \frac{\text{(surface roughness length of new terrain)}}{\text{(surface roughness length of tower area terrain)}}$$

(b) If $m < 1.5$, no changes are necessary. If $m > 1.5$, do not modify the first 4 subsectors beyond the boundary, but reduce the frequency values in each of the more remote subsectors by:

$$f' = f/(1 + 0.0036m)$$

(c) Set to zero all nonzero frequencies in subsectors more distant from the origin than

$$L'_{max} = L_{max}/(1 + 0.0036m),$$

where L_{max} is the distance from the origin to the last nonzero frequency value.

(2) Salt Deposition Table

(a) Carry out step 1(a) as above.

(b) If $m < 1.5$, make no modifications. If $m > 1.5$, do not modify the first four subsectors beyond the boundary, but increase the drift deposition in each more remote subsector by:

$$s' = s\ (1 + 0.0036m),$$

where s' and s represent modified and old salt deposition in $kg/(km^2\text{-month})$.

For this table, the procedure results in slightly more total salt deposition than was contained in the unmodified table, because the increase in salt deposition in intermediate subsectors is not subtracted from more remote subsectors. It gives, therefore, a conservative estimate of the environmental impact of the drift.

Hilly Terrain, (2), (6-8), and (9)

In hilly terrain the flow is, in general, more turbulent than over flat terrain. Therefore, increased plume dispersion rates are expected (except during stable atmospheric conditions) and drift should be deposited closer to the towers.

If the terrain has a gentle, smooth, rolling surface with slopes ≤ 0.25, the plume usually follows the terrain shape, unless the wind speed is very high (6). Output modifications in this case will thus depend on wind speed category.

When the wind speed is low and the flow approaches hilly terrain from flat terrain, the wind speed will increase over the hilly terrain by a recommended ratio of 1.2, (6, p.171). The acceleration is due to gravitational motions up and down the slopes of the hills, (anabatic and katabatic winds).

On the other hand, if the wind speed is high as the flow approches hilly terrain from flat terrain, it becomes weaker by a recomended factor of 0.75. This happens because strong winds are produced by a pressure gradient on a synoptic scale, and the surface geometry is less important in determining the wind speed. The hilly terrain appears only as an increased surface roughness. Thus, when both the tower area and the region over which the plume passes are hilly but the wind data comes from nearby flat terrain, plume lengths will be greater for low wind speeds and less for high wind speeds, because of the corresponding acceleration and deceleration. But for low winds, the plume also has to travel further along the hill slopes to reach a given horizontal distance. Thus, the two effects tend to cancel for low winds.

The recommended steps for modification of the TABLES code output are as follows:

(1) Low-to-moderate slopes ($\leq \frac{1}{4}$).

(a) For low or moderate wind speed, no modification of the tables of plume length or salt deposition are required. To justify this approximation, we appeal to the tendency toward cancellation of the two effects mentioned above.

(b) In the case of high winds, we face two possibilities:

(i) The tower is in flat terrain, the wind data comes from the tower area terrain, and hilly terrain begins within a couple of kilometers, (or the tower is in hilly terrain and flat terrain begins within a couple of kilometers). When a terrain transition occurs within the plume dispersion region, the modifications can be handled as in a change of surface roughness by taking $^1/_3$ of the average hill height as the roughness length in the hilly terrain. However, the table entry changes in each subsector should be reduced by the fraction of high wind cases for that season in that sector, as determined from the frequency tables for wind speed range.

(ii) The tower and plume dispersion region both lie in either flat or hilly terrain, but the wind data comes from a nearby location lying in the other type of terrain. In this case we also suggest treating the modification in the same way as for a change in surface roughness as in (i). But all sectors should be modified and the boundary for terrain roughness change should be taken as the origin for all sectors.

(2) Steep Slopes, ($\geq \frac{1}{4}$)

(a) Low-to-moderate winds. As was mentioned earlier, winds will accelerate over the hilly terrain and plumes will become longer on the average. But because of the steep slopes, diffusion is faster and that shortens the plumes. Therefore, the net effect is treated as producing no change in the plume length frequencies but a slight increase in the salt deposition closer to the towers. The conservative procedure of modifying salt deposition tables when the wind data is taken in the same flat terrain where the towers are located is as follows:

$$s' = s\ [1 + (\text{average slope} - 0.25)],$$

for the subsectors covered by the hilly terrain. This procedure is conservative, introducing more total salt than before modification, because the additional deposition is not removed from more distant

subsectors. If the wind data are taken in the hilly terrain and a cooling tower is also located in hilly terrain, no modifications are required.

(b) High winds. Treat this case as in 1(b).

Uniformly Sloping Terrain, (2), (10)-(12)

Each case of uniformly sloping terrain leads to identification of a direction of steepest ascent or descent and to the computation of the maximum slope angle ϕ. But the centerline for a given wind direction sector being modified will not, in general, lie along the direction of steepest ascent, but at an angle ζ to it in the horizontal plane. As a plume moves down the sector, it will experience a lessened slope angle θ. The formula relating these three angles (shown in Fig. D-4) is:

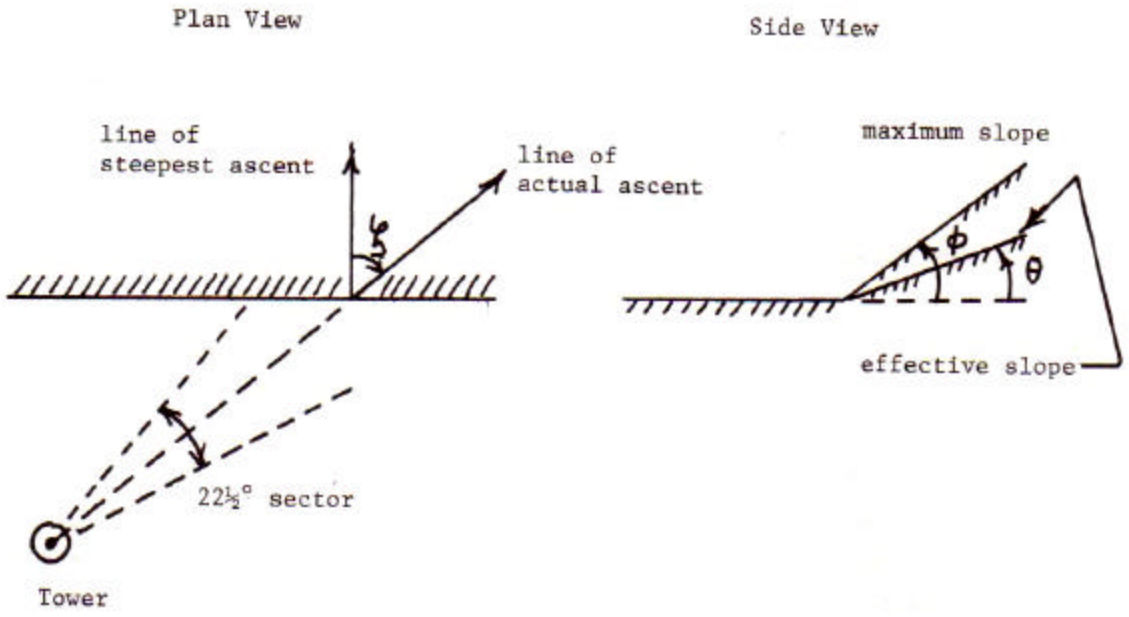

Figure D-4. Geometry for effective slope angle when centerline of subsector makes an angle ζ with the line of steepest ascent (descent).

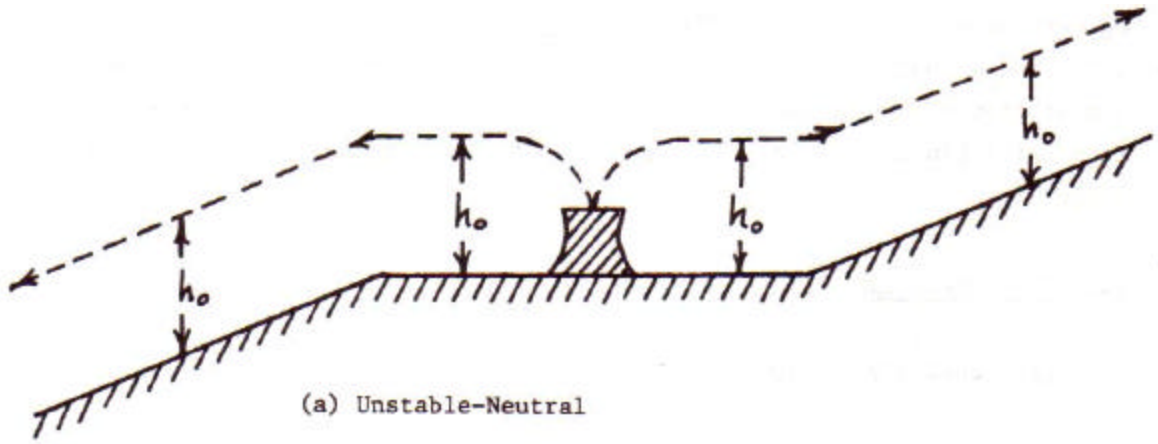

(a) Unstable-Neutral

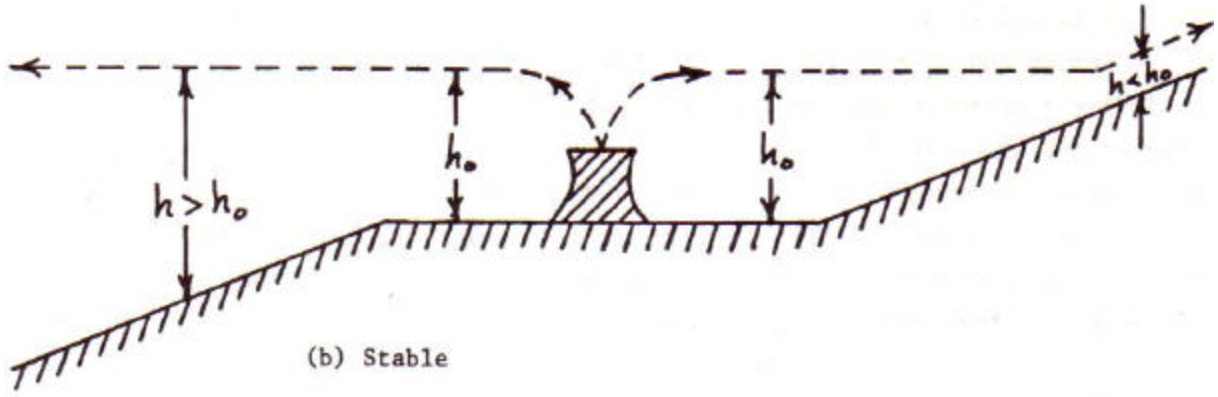

(b) Stable

Figure D-5. Behavior of plume centerline with respect to uniformly sloping terrain as a function of ambient stability.

$$\tan \theta = \tan \phi \, (1 + \tan^2 \zeta)^{-\frac{1}{2}}$$

To illustrate, if $\phi = 20°$, we give below a short table of ζ and effective slope θ values.

ζ	θ
10°	19.7°
30°	17.5°
50°	13.2°
70°	7.1°

A simple model illustrated by Fig. D-5 is proposed for plume behavior in uniformly sloping terrain as suggested in (10). In Fig. D-5(a) covering unstable or neutral cases, the plume centerline follows the terrain either upslope or downslope. In the case of stable stratification the plume centerline stays at a constant absolute elevation until (in the upslope wind case) it impinges on the terrain, as shown in Fig. D-5(b).

(1) Positive Slope.

(a) Unstable-neutral stratification.

The plume stays at constant height above the ground and gains buoyancy as it moves upslope, the effect of which tends to accelerate the plume. On the other hand, there is a loss of kinetic energy due to gravity. Therefore, the two effects tend to cancel each other. Thus we assume that no significant difference in the plume length and no modifications to plume length frequency tables are necessary. A similar argument holds for the salt deposition table. The droplets are at the same height above the terrain as they would be over flat terrain. The droplets have the same amount of time to travel until they hit the ground in reaching a given distance along the terrain. However, in interpreting the resulting isopleths, the terrain slope may need to be considered in establishing the horizontal distance from the tower to a given isopleth. For both types of tables we recommend that the resulting isopleths be interpreted as along the terrain. Because the "tilted" radial intervals are incommensurate with the horizontal radial intervals, we would suggest this reinterpretation rather than a difficult and lengthy recalculation of subsector values.

In summary, the following steps for output modification are proposed for this

(i) plume length tables - no modifications; reinterpretation as along terrain.

(ii) salt deposition tables - no modifications; reinterpretation as along terrain.

(b) Stable stratification.

Since there is an opposite buoyancy effect under stable conditions, the plume travels upslope more slowly than in the previous case. When the winds are low it can even become stagnant. Therefore, the travel time increases which leads to shortening of the plume. Salt deposition also increases nearer the towers, because the droplets have a shorter distance to travel in order to hit the ground, in addition to slower transport speeds along the terrain.

The following steps for output modifications are proposed in this case:

(i) plume length tables - let n be the radial index of the last subsector within the sector under consideration before the sloping terrain begins in that sector. Then there are no modifications for radial subsectors labelled by m for $m \leq n+10$. For $m > n+10$ the subsector plume length frequencies are modified according to:

$$f' = f \cdot \cos\theta_i \cdot \left(\frac{n + 10}{m}\right)^{\frac{1}{2}}$$

where θ_i is the relative angle of the sloping terrain in the i-th sector. (See introduction to this section.)

(ii) Salt deposition tables - let n be the index of the last subsector within the given sector under consideration before the sloping terrain begins in that sector.

- Make no change in s_j for $n < j \leq n + 10$, (500m beyond the boundary)
- Compute

$$D = \sum_{j=n+21}^{50} (2j-1)\, s_j$$

- Add to subsector j, $(n + 10 < j \leq n + 20)$, the deposition rate

$$\Delta s = \frac{D}{20(n+5)}$$

This procedure is conservative. It will increase the total salt deposition after modification because we do not subtract the increased deposition from more remote subsectors $(j > n + 20)$.

(2) Negative Slope

(a) Unstable-neutral stratification.

The plumes will travel at constant height above the terrain and no significant changes in the plume length should be expected. The same argument holds for the salt deposition, as discussed above. As before, the isopleth results should be interpreted as along the terrain. Thus, the recommended changes are:

i) plume length frequency table - no modifications; reinterpretation as along terrain.
ii) salt deposition frequency tables - no modifications; reinterpretation as along terrain.

(b) Stable stratification.

In this case the distance between the plume centerline and the ground increases as the plume travels. Therefore the droplets must travel farther to reach the ground and are deposited further out. We expect no significant changes in the visible plume length, because the plume has the same time to evaporate in traveling to reach a given horizontal distance as it would in the case of flat terrain. In the light of this brief justification, we recommend the following steps in this case:

i) plume length - no modification; interpret isopleths as long the horizontal direction.
ii) salt deposition - Let n be the index of the last non-zero subsector value in the given sector (if there is one). That is, $s_n \neq 0$, but $s_{n+1} = 0$.

- Compute

$$s = \frac{1}{3} \sum_{j=n-2}^{n} s_j.$$

- Replace s_j by s for all the j which satisfy $n-1 < j < n+5$.

- Replace s_j by $s(\cos\theta)$ for $j > n+4$.

If there are no zero values of s_j in the sector being considered, and if m is the index of the last subsector then carry out the following steps:

- Compute

$$s = \frac{1}{3} \sum_{j=m-11}^{m-9} s_j.$$

- Replace s_j by s for all j such that $m-12 < j < m$.

Both procedures in this case are conservative. Both result in increased total salt deposition, and both emphasize the fact that for negative slopes and under stable conditions the droplets are deposited further out than in the case of flat terrain.

Ridge, (12)-(17).

A two-dimensional ridge has been defined above. An average plume opening angle is 19°, which is close to the opening angle of a sector (22.5°). Also we have required a ridge to be at least three sectors wide. Here we note that this requirement is not radius dependent because the plume will remain within a single sector. (Or it will remain within two adjacent sectors if the wind direction is nearly along the boundary direction.) For a wide range of angles (around 90°) between the ridge long axis and sector mean direction, the effects are nearly the same. The sector need not intersect the ridge at right angles to its long dimension for the procedures we will suggest to be valid.

We have concluded from the available data that the plume trajectory usually follows the ridge shape. But it levels off at a slightly higher elevation on the lee side than the elevation at which it approached on the windward side. (That is, h_2 is slightly larger than h_1 in Fig. D-6.)

The streamlines converge above the ridge crest, but the curvature of the steamlines becomes smaller as the difference in height between the plume and the ridge becomes larger, (curvature $\cong (H-h_1)^{-1}$). Convergent streamlines lead to vertical shrinkage of the plume.

Other important features of the flow over a ridge are separation of the flow on the lee side and the generation of lee side vortices. There are many consequences of these features in plume behavior. For example, the generation of vortices causes increased turbulence and increased diffusion and evaporation rates. Drift deposition may be increased due to trapping of droplets in the vortex circulation and due to increased turbulence. These effects are only significant when the ridge height is more than 200m. Ridges (or hills) of steeper slope cause more turbulence and eddy motion than ridges of gentler slope.

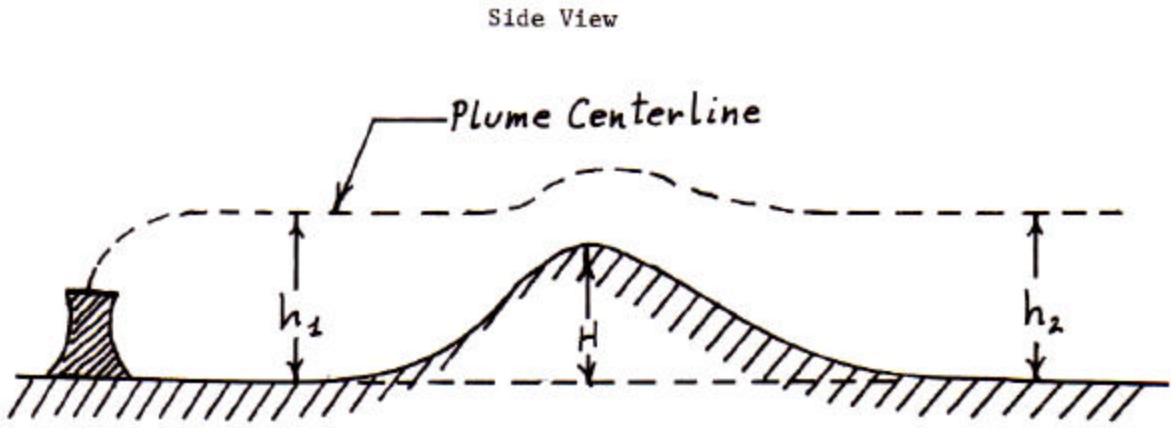

Figure D-6. Typical behavior of the plume centerline as the plume traverses a ridge.

If the ridge elevation is less than 150m above the towers, no modifications are required, because the plume centerline will usually pass well above the top of the ridge. Except when the sector includes a ridge end (which should be treated as a

semi-3D hill) the plume air must pass over the ridge. Mass conservation requires that the flow velocity first increase somewhat on the upslope and then decrease somewhat on the downslope to accomplish this. The time required for a plume parcel to reach a given horizontal distance is thus about the same as in flat terrain with the same wind speed. However, the ridge will usually introduce additional turbulence and mixing into the flow. This tends to shorten the plumes. We suggest no changes to the plume length frequency tables for all stabilities and wind speeds as a conservative procedure.

However, for salt deposition, the presence of the ridge and of lee side turbulence will require changes. Table D-2 directs the user either to leave these tables also unmodified, or to adopt one of two modification procedures under stable conditions depending on wind-speed range. (That is, both procedures must be used and the resulting changes weighted with the appropriate frequencies from the combined ambient condition frequency table entries for the sector).

Table D-2. Procedure selection for a ridge as a function of wind speed range and ambient stability category ("None" means no changes to salt deposition tables).

		Wind Speed Range		
		Low	Moderate	High
Ambient Stability	Unstable	None	None	None
	Neutral	None	None	None
	Stable	A	B	B

A. For stable, low wind conditions we suggest the following changes to the salt deposition tables:

(1) Identify m, the radial index of the last nonzero subsector entry. If R_j is the average radius of radial subsector j, compute

$$\Delta s = \frac{1}{3} \sum_{j=1}^{3} R_{m-j}\, s_{m-j}$$

(In this formula s_j is the drift rate for subsector j.)

(2) If the average radius of a subsector which includes the ridge in the sector under study is R, increase the drift rate in the subsector by:

$$wR^{-1}(\Delta s),$$

where w is the frequency weight in that sector for stable, low wind conditions. Make this change to both windward and lee side subsectors which include the ridge.

B. For stable conditions with moderate to high winds the following steps should be applied to the salt deposition tables:

(1) Compute Δs according to A(1) above.
(2) Add only to every lee side subsector of average radius R an amount

$$wR^{-1}(\Delta s),$$

where w is the frequency weight in that sector for stable conditions with moderate or high wind speeds.

Three-Dimensional Hill, (6), (12), (14), (17)-(21)

The physics of the air flow past a 3D hill depends strongly on stratification and wind speeds, even more so than in the case of a ridge. The approaching air can either go around or over the hill in this case. For a ridge the air usually has to go over the ridge. For example, in the case of stable conditions and small wind speeds, the flow has little kinetic energy and develops no buoyancy on rising Therefore the flow cannot rise up over the hill, but stays horizontal. That is, each air parcel remains in the same horizontal plane, even if it has to go around the hill (14). In the case of this "horizontal flow", the separation of the flow occurs roughly at $\theta \sim 110^{\circ}$, as shown in Fig. D-7.

An opposite case occurs with high wind speeds and unstable conditions. The air flow has a lot of kinetic energy and develops buoyancy on rising. Therefore, all of the air which approaches the hill will go over it. A less clear-cut case would contain unstable conditions and low winds or stable conditions and high winds, where kinetic energy and buoyancy effects compete.

In terms of plume dispersion, when the flow is horizontal, the two halves of the plume will go to the neighboring sectors. In the case of flow over the hill, when the plume impinges on the lower part of the hill, it will spread thinly over the entire hill surface.

Side View

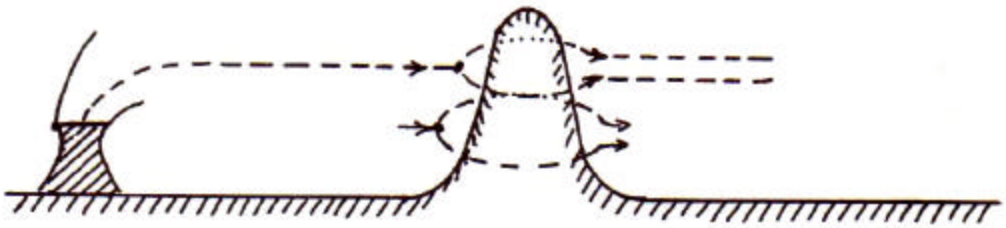

Top View

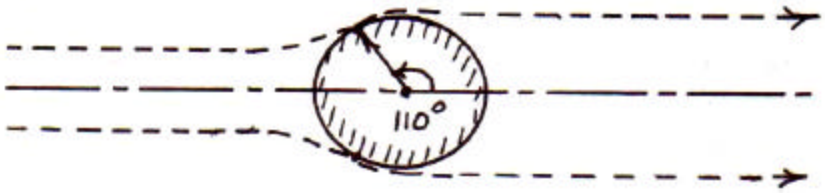

Figure D-7. Flow in a horizontal plane around a hill under low wind and stable ambient conditions.

Thus we have to consider separately two cases, and for each we must establish simple procedures for changing the plume length frequency and salt drift tables. Table D-3 directs the user to the appropriate procedure as a function of stability and wind speed.

Table D-3. Procedure selection for a 3D hill as a function of wind speed range and ambient stability category ("None" means no changes to length or salt deposition tables)

		Wind Speed Range		
		Low	Moderate	High
Ambient Stability	Unstable	B	None	None
	Neutral	B	None	None
	Stable	A	B	B

As concluded earlier, for low wind speeds and stable stratification the flow is completely horizontal. The steps to modify the tables are as follows:

(1) Plume length frequency table.

At most two adjacent sectors can intersect the hill due to the definitions distinguishing a hill from a ridge. We will assume that the hill lies completely in one sector, labelled by i (between 1 and 16), and begins at radial subsector j. Since the basic idea is to move a fraction w_i of the frequency from such subsectors radially to one or both sides to the nearest sectors which do not include the hill, this example illustrates the procedure well enough. (As above, w_i is the frequency weight of stable low wind conditions in sector i). The procedure is to subtract $w_i f_{ij}$ from subsector (i,j) and add 0.5 $w_i f_{ij}$ to subsector (i-1,j) and (i+1,j). This procedure is then repeated for all subsectors labeled by (i,k) with k>j. If the hill only occupies part of the angular extent of a given sector, the frequency to be removed sidewise can be reduced by a further factor obtained by dividing the angular extent of the hill in the sector by 22.5°. If subsectors (i,j) and (i+1,j) both include the hill, then $w_i f_{ij}$ would be moved to (i-1,j) and $w_{i+1}\ f_{i+1,j}$ would be moved to (i+2,j).

(2) Salt deposition tables

Carry out the same steps as in 1) for plume length frequency, where instead of frequencies f, one adjusts salt deposition rates s in kg/(km^2-month). This procedure conserves the total amount of salt. For a conservative estimate of the effects of lee side turbulence or salt deposition, the user can increase s by a factor of 1.2 (6) on the lee side of the hill. But then, of course, the total amount of salt deposited is increased.

winds and stable stratification a mixed procedure is recommended. Reduce by an additional factor of ½ the amount $w_i f_{ij}$ or $w_i s_{ij}$ to be removed from subsector (i,j) sideways according to Procedure A. Here remember that the weight w_i is obtained as the sum of four frequency table entries from the combined frequency table. These four entries are found in rows 1, 4, 8, and 9 of that table, an example of which is shown as Table D-4. In general, the summation of the four frequencies will more than compensate for the additiona factor of ½, so that Procedure B will result in at least as much adjustment

Table D-4. Frequency factors by wind direction for stability class, wind speed range and combined stability class and wind speed range.

STABILITY CLASS BY WIND DIRECTION
LINEAR MECHANICAL DRAFT COOLING TOWER -- DUAL LINE ARRAY CONFIGURATION
SEASON=ANNUAL

STABILITY CLASS	WIND FROM																
	N	NNE	NE	ENE	E	ESE	SE	SSE	S	SSW	SW	WSW	W	WNW	NW	NNW	
	PLUME HEADED																
	S	SSW	SW	WSW	W	WNW	NW	NNW	N	NNE	NE	ENE	E	ESE	SE	SSE	STAB.
1	0.01	0.0	0.0	0.00	0.01	0.0	0.01	0.00	0.00	0.00	0.00	0.00	0.00	0.00	0.01	0.00	0.0
2	0.02	0.02	0.03	0.05	0.03	0.05	0.02	0.02	0.02	0.02	0.02	0.04	0.04	0.03	0.02	0.01	0.06
3	0.07	0.08	0.11	0.10	0.12	0.11	0.05	0.09	0.08	0.09	0.11	0.12	0.09	0.09	0.07	0.03	0.11
4	0.57	0.73	0.67	0.58	0.53	0.37	0.46	0.56	0.63	0.70	0.72	0.62	0.60	0.56	0.69	0.72	0.06
5	0.20	0.11	0.11	0.13	0.19	0.25	0.21	0.22	0.21	0.13	0.11	0.15	0.18	0.22	0.13	0.14	0.13
6	0.11	0.05	0.06	0.09	0.09	0.19	0.22	0.08	0.05	0.05	0.04	0.06	0.07	0.08	0.08	0.08	0.28
7	0.02	0.01	0.01	0.03	0.03	0.03	0.04	0.01	0.01	0.01	0.01	0.01	0.02	0.01	0.01	0.01	0.36

WIND SPEED DISTRIBUTION BY DIRECTION AT REFERENCE HEIGHT OF 200 METERS
LINEAR MECHANICAL DRAFT COOLING TOWER -- DUAL LINE ARRAY CONFIGURATION
SEASON=ANNUAL

WIND RANGE	WIND FROM																
	N	NNE	NE	ENE	E	ESE	SE	SSE	S	SSW	SW	WSW	W	WNW	NW	NNW	
	PLUME HEADED																
	S	SSW	SW	WSW	W	WNW	NW	NNW	N	NNE	NE	ENE	E	ESE	SE	SSE	STAB.
1	0.03	0.01	0.02	0.02	0.02	0.03	0.04	0.01	0.01	0.00	0.00	0.01	0.01	0.01	0.01	0.01	1.00
2	0.13	0.07	0.10	0.20	0.12	0.26	0.26	0.11	0.07	0.06	0.08	0.10	0.12	0.10	0.13	0.08	0.0
3	0.84	0.92	0.88	0.78	0.86	0.70	0.70	0.88	0.92	0.94	0.91	0.89	0.87	0.88	0.86	0.91	0.0

COMBINED FACTORS BY WIND DIRECTION
LINEAR MECHANICAL DRAFT COOLING TOWER -- DUAL LINE ARRAY CONFIGURATION
SEASON=ANNUAL

COMBINED CLASS*	WIND FROM																
	N	NNE	NE	ENE	E	ESE	SE	SSE	S	SSW	SW	WSW	W	WNW	NW	NNW	
	PLUME HEADED																
	S	SSW	SW	WSW	W	WNW	NW	NNW	N	NNE	NE	ENE	E	ESE	SE	SSE	STAB.
1	0.00	0.00	0.00	0.00	0.00	0.01	0.00	0.00	0.00	0.00	0.00	0.00	0.00	0.00	0.00	0.00	0.17
2	0.01	0.01	0.02	0.03	0.02	0.04	0.02	0.01	0.01	0.01	0.01	0.02	0.02	0.01	0.01	0.00	0.0
3	0.08	0.10	0.13	0.13	0.14	0.11	0.05	0.11	0.09	0.10	0.12	0.14	0.11	0.11	0.08	0.04	0.0
4	0.02	0.01	0.01	0.02	0.01	0.02	0.03	0.01	0.01	0.00	0.00	0.01	0.01	0.01	0.01	0.01	0.19
5	0.10	0.06	0.08	0.14	0.09	0.16	0.17	0.09	0.06	0.05	0.07	0.07	0.09	0.08	0.10	0.07	0.0
6	0.65	0.76	0.69	0.56	0.62	0.44	0.47	0.69	0.78	0.78	0.75	0.68	0.68	0.70	0.71	0.79	0.0
7	0.00	0.00	0.00	0.00	0.00	0.01	0.01	0.00	0.00	0.00	0.00	0.00	0.00	0.00	0.00	0.00	0.64
8	0.02	0.00	0.01	0.02	0.01	0.06	0.07	0.01	0.00	0.00	0.00	0.01	0.01	0.01	0.01	0.01	0.0
9	0.11	0.06	0.06	0.09	0.10	0.16	0.18	0.08	0.06	0.05	0.05	0.06	0.08	0.08	0.07	0.08	0.0

* COMBINED CLASSES ARE DEFINED AS FOLLOWS:
1=UNSTABLE, LOW WIND 2=UNSTABLE, MODERATE WIND 3=UNSTABLE, HIGH WIND
4=NEUTRAL, LOW WIND 5=NEUTRAL MODERATE WIND 6=NEUTRAL, HIGH WIND
7=STABLE, LOW WIND 8=STABLE, MODERATE WIND 9=STABLE, HIGH WIND

REFERENCES

1. T. Tesche. Private Communication. Systems Application, Inc., San Rafael, CA. July 1982.

2. W. Frost and D.K. Nowak. Summary and Guidelines for Siting Wind Turbine Generators Relative to Small-scale Two-dimensional Terrain Features. U.S. Department of Energy, RLO-2443-77/1. March 1979.

3. E.J. Plate. Aerodynamic Characteristics of Atmospheric Boundary Layers. U.S. Atomic Energy Commission. 1971.

4. H.A. Panofsky. The Atmospheric Boundary Layer Below 150 Meters. Annual Review of Fluid Mechanics. 1974.

5. K.S. Rao, J.C. Wyngaard and O.R. Cote. The Structure of the Two-dimensional Internal Boundary Layer Over a Sudden Change in Surface Roughness. J. Atm. Science, 31. 1974, pp 738-746.

6. W. Frost and C.F. Shieh. Guidelines for Siting WECS Relative to Small-scale Terrain Features. U.S. Department of Energy, DOE/ET/20242-78/1. December 1981.

7. J. Frenkel. Wind Profiles Over Hills. Quarterly Journal of the Royal Meteorological Society, 88. 1961, pp. 156-169.

8. R.C. Koch, et. al. Power Plant Stack Plumes in Complex Terrain: An Appraisal of Current Research. Environmental Protection Agency. EPA-600/7-77-020. March 1977.

9. H.M. Ellis and P.C. Liu. Comparison of Predicted and Measured Concentrations for 54 Alternative Models of Plume Transport in Complex Terrain. 72nd Annual Meeting of Air Pollution Control Association. June 1979.

10. Valley Model User's Guide. U.S. Environmental Protection Agency, EPA-450/2-77-018. 1977.

11. K.E. Pickering, R.H. Woodward, and R.C. Koch. Power Plant Stack Plumes in Complex Terrain. Data Analysis and Characterization of Plume Behavior. U.S. Environmental Protection Agency, EPA-600/7-80-008. January 1980.

12. World Meteorological Organization. Air Flow Over Mountains. Technical Note No. 34, WMO-NO. 98. 1960, p. 43.

13. R.D. Rowe, C.Z. Lee, and J.J. Haulena. The Elevation of Stable Atmospheric Plumes Above a Ridge. 73rd Annual Meeting of the Air Pollution Control Association, Montreal, Quebec, 80-55.5. June 1980.

14. Y. Lee. Concentration in the Lee of a Mountain for Stable Airflow over a Mountain Ridge. Proceedings of the Second Joint Conference on Applications of Air Pollution Meteorology. American Meteorological Society, New Orleans, Louisiana. 1980.

15. L.H. Khurshudyan, W.H. Snyder, and I.V. Nekrasov. Flow and Dispersion of Pollutants Over Two-dimensional Hills: Summary Report on Joint Soviet-American Study. U.S. Environmental Protection Agency, EPA-600/4-81-067. August 1981.

16. A.H. Huber, W.H Snyder, and R.E. Lawson. Stack Placement in the Lee of a Mountain Ridge: A Wind Tunnel Study. U.S. Environmental Protection Agency, EPA-600/4-76-047. September 1976.

17. W. Eberhard. Field Measurements in Support of Dispersion Modeling in Complex Terrain. NOAA Technical Report Memorandum, ERL WPL-78, (PB82-148644). July 1981.

18. J. Hunt, W. Snyder, and R. Lawson. Flow Structure and Turbulent Diffusion Around a Three-dimensional Hill. U.S. Environmental Protection Agency, EPA-600/4-78-041. 1978.

19. J. Hunt and W. Snyder. Experiments on Stably and Neutrally Stratified Flow Over a Three-dimensional Hill. J. Fluid Mechanics, 96, Part 4. 1980.

20. G.P. Crapper. Waves in the Lee of a Mountain with Elliptical Contours. Phil. Trans. Roy. Soc., A254. 1962, pp. 601, 623.

21. R.I. Sykes. Stratification Effects in Boundary Layer Flow over Hills. Proc. Roy. Soc., A-261. 1978, p. 275.